

(NASA-CR-148718) USE OF STEEPEST DESCENT
AND VARIOUS APPROXIMATIONS FOR EFFICIENT
COMPUTATION OF MINIMUM NOISE AIRCRAFT
LANDING TRAJECTORIES Annual Report
(Virginia Univ.) 85 p HC \$5.00

N76-3091

Unclas
48753

CSCI 20A G3/71

USE OF STEEPEST DESCENT AND VARIOUS APPROXIMATIONS
FOR EFFICIENT COMPUTATION OF MINIMUM NOISE
AIRCRAFT LANDING TRAJECTORIES

Annual Report

Contract No. NSG 1101

Submitted to:

NASA Scientific & Technical Information Facility
P. O. Box 8757
Baltimore/Washington International Airport
Maryland 21240

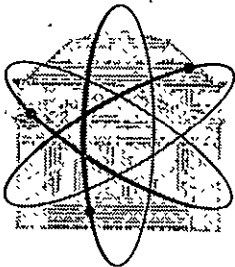
Submitted by:

G. Cook
Professor

R. M. Witt
Research Assistant

SCHOOL OF ENGINEERING AND
APPLIED SCIENCE

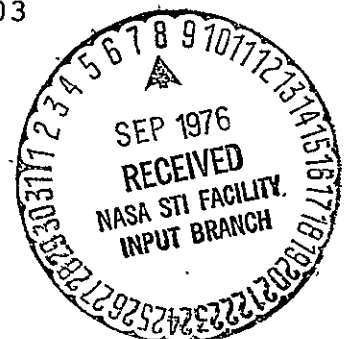
RESEARCH LABORATORIES FOR THE ENGINEERING SCIENCES



UNIVERSITY OF VIRGINIA
CHARLOTTESVILLE, VIRGINIA 22901

Report No. UVA/528075/EE76/103

August 1976



RESEARCH LABORATORIES FOR THE ENGINEERING SCIENCES

The School of Engineering and Applied Science of the University of Virginia has long believed that strong research capabilities go hand in hand with effective teaching. Early in the development of its graduate training program, the School also recognized that men and women engaged in research should be as free as possible of the administrative chores involved in sponsored research. In 1959, therefore, the Research Laboratories for the Engineering Sciences (RLES) was established and assigned the administrative responsibility for such research within the School.

Currently, approximately 60 members of the faculty, who also teach at the undergraduate and graduate levels, and 30 additional professional engineers and scientists, whose primary responsibility is research, generate and conduct the investigations that make up a vigorous and wide-ranging program. The Director of RLES, a faculty member and active researcher himself, maintains familiarity with the support requirements of all research under way. He is aided by an RLES Academic Advisory Committee made up of one faculty representative from each academic department of the School. This Committee serves to inform RLES of the needs and perspectives of the research community.

In addition to administrative support, RLES is charged with providing technical assistance where it is needed. Because it is not practical for each department of the School to become self-sufficient in all phases of the supporting technology essential to present-day research, RLES makes services available through the following support groups: Machine Shop, Instrumentation, Facilities Services, Publications (including photographic facilities), and Computer Terminal Maintenance.

The purpose of RLES, then, is to provide administrative and technical assistance for sponsored research carried out within the School of Engineering and Applied Science of the University of Virginia. Such research has played an important part in the University's contribution to scientific knowledge and service to the community and continues the successful partnership of University, government, and industry.

For information on current programs and capabilities, write to Director, Research Laboratories for the Engineering Sciences, Thornton Hall, University of Virginia, Charlottesville, Virginia 22901.

USE OF STEEPEST DESCENT AND VARIOUS APPROXIMATIONS
FOR EFFICIENT COMPUTATION OF MINIMUM NOISE
AIRCRAFT LANDING TRAJECTORIES

Annual Report

Contract No. NSG 1101

Submitted to:

NASA Scientific & Technical Information Facility
P. O. Box 8757
Baltimore/Washington International Airport
Maryland 21240

Submitted by:

G. Cook
Professor

R. M. Witt
Research Assistant

Department of Electrical Engineering
RESEARCH LABORATORIES FOR THE ENGINEERING SCIENCES
SCHOOL OF ENGINEERING AND APPLIED SCIENCE
UNIVERSITY OF VIRGINIA
CHARLOTTESVILLE, VIRGINIA

Report No. UVA/528075/EE76/103
August 1976

Copy No. 1

TABLE OF CONTENTS

Section	Page
FOREWORD	1
I. INTRODUCTION	2
II. GENERAL SYSTEM EQUATIONS	4
2.1 INTRODUCTION	4
2.2 SYSTEM EQUATIONS	8
2.3 INTEGRATION METHOD	11
2.3.1 RUNGE-KUTTA FOURTH ORDER	11
2.3.2 MILNE-REYNOLD'S	13
2.4 SUMMARY	14
III. AIRCRAFT MODEL	15
3.1 INTRODUCTION	15
3.2 SOURCE OF DATA	15
3.3 STABILITY DERIVATIVE SIMULATION	17
3.3.1 DIRECT DATA STORAGE	17
3.3.2 FUNCTIONAL APPROXIMATION	19
3.3.3 CHOICE OF REPRESENTATION	26
3.3.4 IMPLEMENTATION	26
3.4 MODEL RESTRICTIONS	29
3.5 AIRCRAFT STATE CONSTRAINTS	33
3.5.1 MAXIMUM ASCENT AND DESCENT RATES	33
3.5.2 ALTITUDE CONSTRAINTS	34
3.5.3 LOAD FACTOR	35
3.5.4 STALL AND BUFFET	35

Section	Page
3.5.5 ANGLE OF ATTACK	39
3.6 AIRCRAFT CONTROL SURFACE CONSTRAINTS	41
3.7 AIRCRAFT ENGINE CONSTRAINTS	44
3.7.1 OPERATIONAL LIMITS	44
3.7.2 FUEL CONSUMPTION MODEL	49
3.8 MODEL ACCURACY	56
3.9 SUMMARY	66
IV. PROGRAMMING THE STEEPEST DESCENT OPTIMIZATION PROCEDURE	67
4.1 INTRODUCTION	67
4.2 PROBLEM AREAS	67
4.3 PROGRAM SIZE AND COST	69
V. RESULTS	70
5.1 INTRODUCTION	70
5.2 PATTERN OF CONVERGENCE	72
VI. CONCLUSIONS AND FUTURE PLANS	75
VII. REFERENCES	76

LIST OF TABLES

Table	Page
I. Abscissa Uniform Interval Sizes and Ranges Used in Direct Data Computer Storage Estimate	19
II. Effect on Performance of Constant Aircraft Weight and Moments of Inertia Assumption	31
III. Maximum Control Deflections and Actuation Rates .	41
IV. Flap Operation Times	43
V. Aircraft Characteristics and States for Four Trajectories	57
VI. Comparison of the Lift Coefficients of the Model and the Original Data	58
VII. Comparison of the Drag Coefficients of the Model and the Original Data	60
VIII. Comparison of the Lateral Forces Coefficients of the Model and the Original Data	61
IX. Comparison of the Pitch Coefficients of the Model and the Original Data	62
X. Comparison of the Roll Coefficients of the Model and the Original Data	63
XI. Comparison of the Yaw Coefficients of the Model and the Original Data	64
XII. Results of Ten Iterations on a Four-Mile Trajectory	71

LIST OF FIGURES

Figure		Page
2.1	Coordinate System Relationships	5
2.2	System Equations Solution Flowchart	7
3.1	Boeing 737-100 Configuration	16
3.2	Basic Lift Coefficient	18
3.3	Comparison of Least-Squares Fitted Polynomials with Original Data	21
3.4	Variation of the Pitching Moment Coefficient for Changes in the Pitch Rate	22
3.5	Piecewise Fitted Polynomial	25
3.6	Aerodynamic Data Sign Convention	28
3.7	Load Factor Limit for Flaps Up	36
3.8	Load Factor Limit for Flaps Down	36
3.9	Stall Speed Characteristics	37
3.10	Low Speed Buffet Angle of Attack	37
3.11	High Speed Buffet Lift Coefficient	40
3.12	Engine Deceleration Characteristics	46
3.13	Engine Acceleration Characteristics	48
3.14	Thrust Specific Fuel Consumption at Sea Level	51
3.15	Thrust Specific Fuel Consumption at 5,000 Feet	52
3.16	Thrust Specific Fuel Consumption at 10,000 Feet	53
5.1	Result of Ten Iterations on a Four-Mile Trajectory	74

LIST OF SYMBOLS

Symbol	Definition
a	Speed of sound
\bar{A}	Coordinate transformation matrix; acceleration, ft/sec ²
(a,b,c)	Ellipsoid semi-major and semi-minor lengths, ft.
b	Wing span, ft.
\bar{c}	Mean chord length, ft.
cg	Center of gravity position, % of \bar{c}
C_L, C_D, C_Y	Total lift, drag, lateral force coefficients
C_l, C_m, C_n	Total roll, pitch, yaw moment coefficients
$C_{L_{Basic}}$	Basic lift coefficient
C_{Lp}	High speed buffet lift coefficient
CPA	Closest point of approach, ft.
d	Distance from (x_E^i, y_E) to L line
f_i	State variable derivative ($i=1,2,\dots,13$)
F	Force, lbs.
F_n	Net thrust, lbs.
g	Gravity acceleration, ft/sec ²
h	Altitude, ft.
h_{min}	Minimum altitude constraint, ft.
h_{max}	Maximum altitude constraint, ft.
$h_{airport}$	Airport sea mean level altitude, ft.

LIST OF SYMBOLS

Symbol	Definition
I	Aircraft moments of inertia, slug-ft ²
K	Aircraft displacement vector in earth fixed system
\overline{J}	Performance index
K_i	Performance index scaling factors
$k_{\delta sp}$	Spoiler panel effectiveness factor
$k_{\delta a}$	Aileron effectiveness factor
L^*	Projection length of principal axes on $Z=0$ plane, ft.
L^{**}	Projection length of principal axes on Z_H axis, ft.
L	Line of intersection of X-Z plane with $Z_E=0$ plane
L, M, N	Roll, pitch, yaw moments, ft-lbs
M	Mach number; ellipsoid principal axes matrix
m	Aircraft mass, lbs.
N_i	Population density, people/mi ²
n_z	Load factor
p, q, r	Roll, pitch, yaw rates, rad/sec
s_p	Trim wheel displacement, deg
s	Wing area, ft ² ; displacement vector of local principal axes from principal axes
T'	Acceleration (deceleration) constraint thrust, lbs
$TFSC$	Thrust specific fuel consumption, lb/hr/lbf
T	Thrust, lbs

LIST OF SYMBOLS

Symbol :	Definition
t	Time,seconds
V	True airspeed,ft/sec
W	Aircraft weight,lbs
Y_{min},Y_{max}	Minimum (maximum) value of Y_E on a noise contour, ft.
X_i	State variable ($i=1,2,\dots,13$)
X,Y,Z	Body axes coordinates,ft.
(x_E^i,y_E)	Coordinates of a point on the noise contour,ft.
α	Angle of attack,rad
β	Sideslip angle,rad
T	Transformation matrix (body-earth fixed)
δ_a	Aileron deflection,deg
δ_e	Elevator deflection,deg
δ_r	Rudder deflection,deg
δ_s	Stabilizer deflection,deg
(ϕ,θ, γ)	Roll,pitch, yaw angles of the aircraft,deg
λ	Eigenvalue of p matrix
ρ	Atmospheric density,slugs/ft ³

FOREWORD

This report covers the third year of a research effort devoted to the determination of minimum noise aircraft landing trajectories. Increased concern for environmental protection, as well as improved measurement and instrumentation capabilities, have provided the primary impetus for this work. Our study has been concerned with the Boeing 737, a short-haul passenger aircraft, and the Patrick Henry Airport which is located at Newport News.

During the three years for which this research has been in progress, we have employed in addition to the principal investigator one post-doctoral researcher and one masters candidate who just received his degree. Also, another masters student has been employed part-time during one summer.

Besides the three annual reports, there have been two technical papers written on our work. One of these has been published and the second one is being reviewed.

Our goal is a working computerized optimization program which may be modified by changing the population data to yield optimal trajectories for any airport. This report gives the current status of the effort.

I. INTRODUCTION

The objective of this report is to bring the reader up to date on the present status of our landing trajectory optimization research without repeating a great deal of what has already been reported in the reports [1,2] on the effort during the first two years.

The accomplishments during the first two years included the following:

1. Develop the aircraft equations.
2. Adapt wind-tunnel data for computer usage.
3. Obtain a passenger comfort model.
4. Develop a noise model.
5. Develop a population model.
6. Integrate the noise model and population model.
7. Establish a performance measure.
8. Use the performance measure to compare constant glide slope trajectories.
9. Set up the equations for the steepest descent optimization procedure.

Each of these items, except number 2, has been discussed in detail in the two previous annual reports. For completeness, discussion of this item will be included here. In addition, the report covers the accomplishments of the past year which are the following:

1. Programming and modifying the steepest descent optimization procedure.

2. Successfully iterating toward the optimum for a four-mile trajectory.
3. Beginning optimization runs for a twenty-mile trajectory.

For reference the two technical papers which we have written are included in the bibliography [3,4].

II. GENERAL SYSTEM EQUATIONS

2.1 Introduction

For the discussion on our treatment of the wind tunnel data to be meaningful, one must have in mind how these data are to be used. Thus, a brief description of our simulation, along with definitions of the variables, seems in order. The realistic simulation of aircraft behavior necessitates the solution to the nonlinear, differential equations of motion. These equations have been formulated as first-order derivatives of the state variables, and they describe the complete six degrees-of-freedom of an actual aircraft.

The equations of motion can have many forms; the specific form depends upon the choice of the coordinate system. Figure 2.1 illustrates the relative orientation between three possible systems. The origin of each of the systems is the aircraft center of gravity.

The body axes (X,Y,Z) are rigidly fixed to the aircraft. The Y axis is perpendicular to the aircraft's plane of symmetry and is directed out the right wing. The X axis is in the plane of symmetry and points toward the front of the aircraft. The Z axis is normal to the X-Y plane and forms a right-handed system. The fuselage reference line (FRL) coincides with the X axis.

The stability axes differ from the body axes by the angle of attack (α_{FRL}). The X_s axis lies in the plane defined by the relative wind vector and the Y body axis, the latter coinciding with the Y_s axis. The Z_s axis is

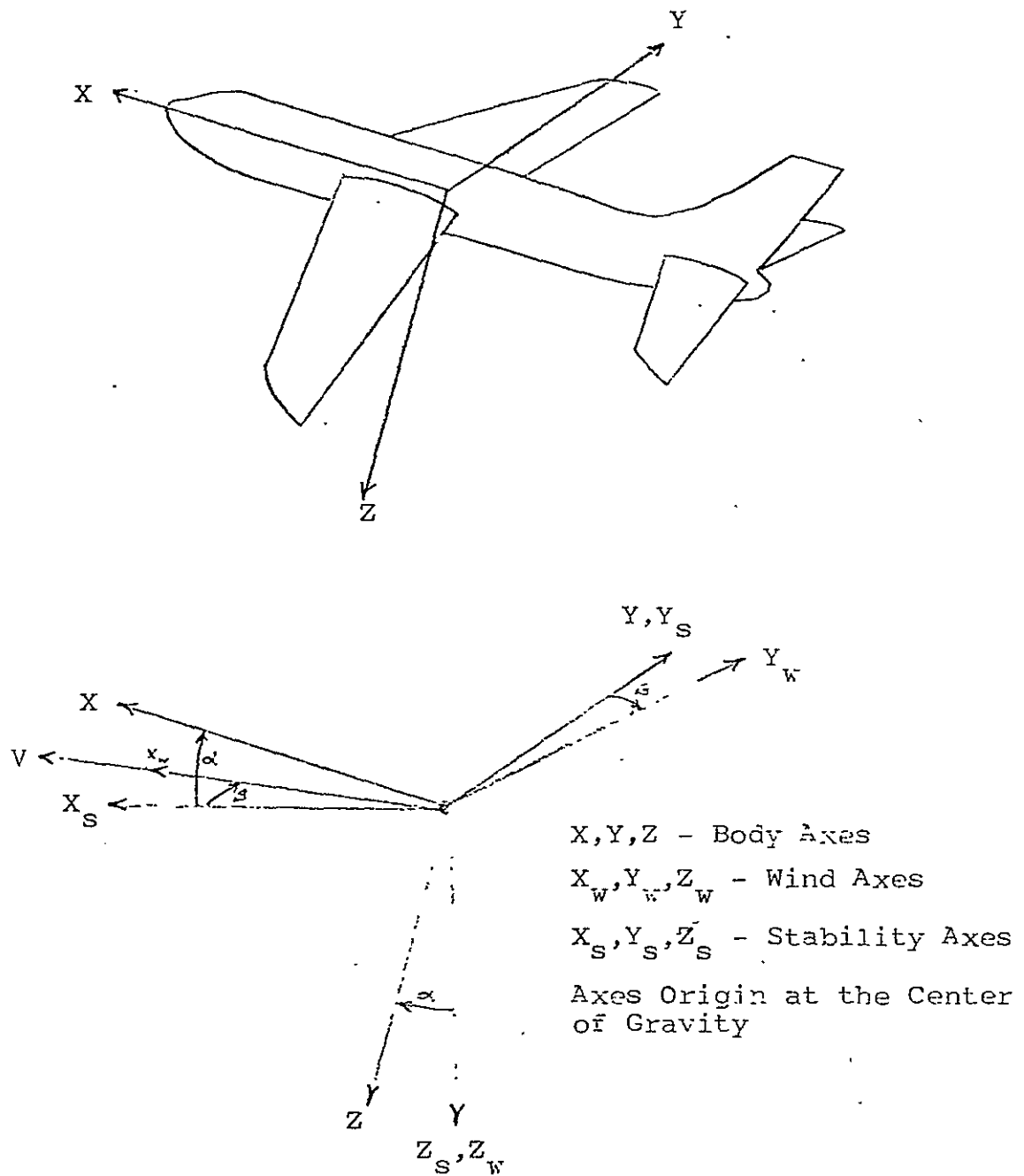


Figure 2.1

Coordinate System Relationships

perpendicular to the X_S - Y_S plane and forms a right-handed system.

The wind axes have the X_W axis collinear with the relative wind vector and differs from the X_S axis by the side-slip angle (β). The Z_W axis coincides with the Z_S axis and Y_W is normal to the X_W - Z_W plane.

The body axes representation yields simple expressions for the Euler angles of the aircraft. However, the relative wind vector, glide slope, angle of attack, and side-slip angle are more difficult to calculate. The wind axes permit simple calculation of the translational equations, angle of attack, and side-slip angle. The disadvantage lies in the complexity of the moment equations and the variable inertia values.

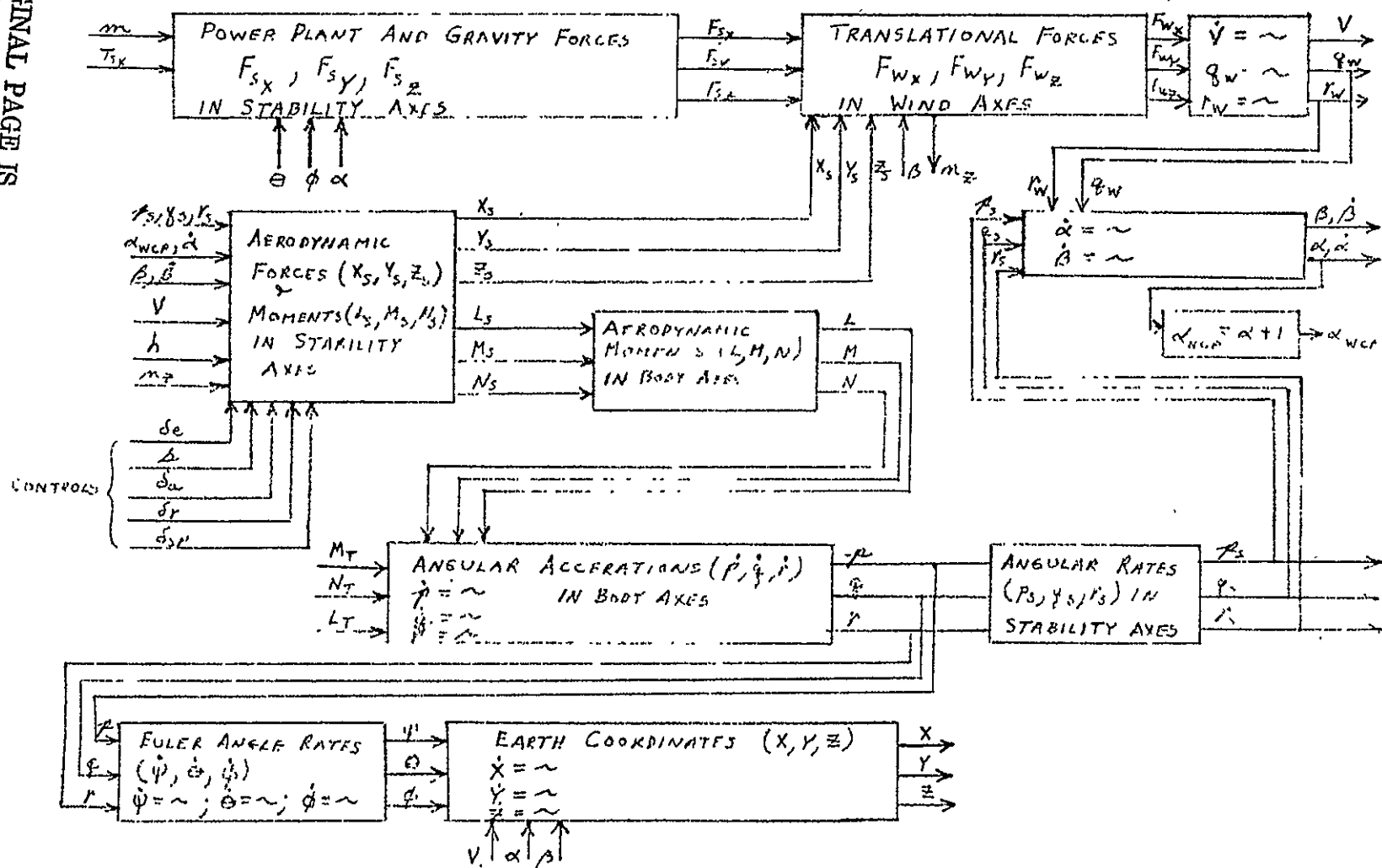
To minimize the complexity of the model, a combination of wind and body axes is used [5]. The translational equations are solved in the wind axes, and the rotational equations are solved in the body axes. The flight path coordinates require the transformation from the body to the earth-fixed axes.

The earth-fixed axes have the X_E and Y_E axes mutually perpendicular, located in the ground plane. The Z_E axis is directed normally into the ground. The center of this system is dependent upon the population model.

The aerodynamic data for the aircraft being modeled was obtained using the stability axes system. This system permits the simple derivation of the aerodynamic forces and

Figure 2.2

System Equations Solution Flowchart



moments. These forces and moments must be resolved into the appropriate system for use in the equations of motion.

Figure 2.2 is a flowchart of the sequence used to solve these equations. This sequence is outlined in the following section.

2.2) System Equations [6,7]

The sequence begins by expressing the thrust vector from each engine in terms of stability coordinates.

$$\begin{aligned}
 T &= F_{n_1} + F_{n_2} \\
 T_{s_x} &= T \cos \alpha_{WCP} \\
 T_{s_y} &= 0 \\
 T_{s_z} &= -T \sin \alpha_{WCP} \\
 \alpha_{WCP} &= \alpha_{FRL} + 1
 \end{aligned} \tag{2.1}$$

The thrust vectors were assumed to be parallel and of equal magnitude. The angle of attack of the engines is the same as that of the wing chord plane (WCP). The moments induced by the thrust vectors are determined in the body axes.

$$\begin{aligned}
 L_T &= N_T = 0 \\
 M_T &= T Z_e
 \end{aligned} \tag{2.2}$$

The load factor is also evaluated.

$$n_z = -(Z_s + T_{s_z}) / mg \tag{2.3}$$

Next, the gravity forces are resolved into components in the stability axes.

$$\begin{aligned}
F_{G_x} &= W (\cos\theta \cos\phi \sin\alpha_{FRL} - \sin\theta \cos\alpha_{FRL}) \\
F_{G_y} &= W \cos\theta \sin\phi \\
F_{G_z} &= W (\sin\theta \sin\alpha_{FRL} + \cos\theta \cos\phi \cos\alpha_{FRL})
\end{aligned} \tag{2.4}$$

The angular velocity components of the aircraft are then expressed in the stability axes.

$$\begin{aligned}
p_s &= p \cos\alpha_{FRL} + r \sin\alpha_{FRL} \\
q_s &= q \\
r_s &= -p \sin\alpha_{FRL} + r \cos\alpha_{FRL}
\end{aligned} \tag{2.5}$$

The aerodynamic forces and moments are calculated in the stability axes system. These forces are then combined with the thrust and gravity forces and transformed into the wind axes system.

$$\begin{aligned}
F_{W_x} &= (T_{S_x} + F_{G_x} + X_s) \cos\beta + (F_{G_y} + Y_s) \sin\beta \\
F_{W_y} &= (F_{G_y} + Y_s) \cos\beta - (T_{S_x} + F_{G_x} + X_s) \sin\beta \\
F_{W_z} &= T_{S_z} + F_{G_z} + Z_s
\end{aligned} \tag{2.6}$$

This is followed by the integration of the velocity, angle of attack, and sideslip angle.

$$\begin{aligned}
\dot{f}_1 &= \dot{V} = F_{W_x} / m \\
\dot{f}_2 &= \dot{\alpha} = (-q_w / \cos\beta) - p_s \tan\beta + q_s \\
\dot{f}_3 &= \dot{\beta} = r_w - r_s
\end{aligned} \tag{2.7}$$

where

$$\begin{aligned}
q_w &= -F_{W_z} / mV \\
r_w &= F_{W_y} / mV
\end{aligned}$$

The aerodynamic moments are then transformed to the body axes system.

$$\begin{aligned} L &= L_S \cos \alpha_{FRL} - N_S \sin \alpha_{FRL} \\ M &= M_S \\ N &= L_S \sin \alpha_{FRL} + N_S \cos \alpha_{FRL} \end{aligned} \quad (2.8)$$

The usual form of the roll, pitch, and yaw moment equations is

$$\begin{aligned} I_{xx} \dot{f}_4 &= I_{xx} \dot{p} = (I_{yy} - I_{zz}) qr + I_{xz} (\dot{r} + pq) \\ &\quad + L + L_T \\ I_{yy} \dot{f}_5 &= I_{yy} \dot{q} = (I_{zz} - I_{xx}) rp + I_{xz} (r^2 - p^2) \\ &\quad + M + M_T \\ I_{zz} \dot{f}_6 &= I_{zz} \dot{r} = (I_{xx} - I_{yy}) pq + I_{xz} (\dot{p} - qr) \\ &\quad + N + N_T. \end{aligned} \quad (2.9)$$

Equation (2.9a) contains an undesirable derivative (\dot{r}) in the right hand side. To eliminate this derivative, equation (c) was substituted into (a). The final form of the equations is

$$\begin{aligned} (I_{xx} I_{zz} - I_{xz}^2) \dot{f}_4 &= (I_{yy} I_{zz} - I_{xz}^2 - I_{zz}^2) qr \\ &\quad + (I_{zz} + I_{xx} - I_{yy}) I_{xz} pq \\ &\quad + (I_{zz} (L + L_T) / I_{xz} (N + N_T)) \\ I_{yy} \dot{f}_5 &= (I_{zz} - I_{xx}) rp + I_{xz} (r^2 - p^2) + M + M_T \\ I_{zz} \dot{f}_6 &= (I_{xx} - I_{yy}) pq + I_{xz} (\dot{p} - qr) + N + N_T. \end{aligned} \quad (2.10)$$

Next, the Euler angular rates are integrated.

$$\begin{aligned} \dot{f}_7 &= \dot{\psi} = (r \cos \phi + q \sin \phi) / \cos \phi \\ \dot{f}_8 &= \dot{\theta} = q \cos \phi - r \sin \phi \end{aligned} \quad (2.11)$$

$$f_9 = \dot{\phi} = p + f_7 \sin\theta$$

Integration of the aircraft velocity components in the earth-fixed axes is the next step.

$$\begin{aligned} f_{10} = \dot{X}_E &= V(\cos\alpha_{FRL}\cos\beta\cos\theta\cos\psi + \sin\beta(-\cos\phi\sin\psi \\ &\quad + \sin\phi\sin\theta\cos\psi) + \sin\alpha_{FRL}\cos\beta(\sin\phi\sin\psi \\ &\quad + \cos\phi\sin\theta\cos\psi)) \\ f_{11} = \dot{Y}_E &= V(\cos\alpha_{FRL}\cos\beta\cos\theta\sin\psi + \sin\beta(\cos\phi\cos\psi \\ &\quad + \sin\phi\sin\theta\sin\psi) + \sin\alpha_{FRL}\cos\beta(-\sin\phi\cos\psi \\ &\quad + \cos\phi\sin\theta\sin\psi)) \end{aligned} \quad (2.12)$$

$$\begin{aligned} f_{12} = \dot{Z}_E &= V(\cos\alpha_{FRL}\cos\beta\sin\theta - \sin\beta(\sin\phi\cos\theta) \\ &\quad - \sin\alpha_{FRL}\cos\beta\cos\theta\cos\phi) \end{aligned}$$

An additional differential equation was included into the system for the performance index. It has the form

$$f_{13} = \dot{J} = K_1 \dot{W}_f + K_2 P + K_3 + \text{PENALTY FUNCTIONS.} \quad (2.13)$$

where the K_i 's are scaling constants, \dot{W}_f is the fuel consumption rate, and P is the instantaneous population exposed to noise. The constant K_3 is the constant for the time component of the performance index.

2.3) Integration Method

2.3.1) Runge-Kutta Fourth Order

An examination of the differential equations (2.7), (2.10), (2.11), (2.12), and (2.13) reveals that they are highly nonlinear and require numerical integration. The

original method employed was a Runge-Kutta fourth order algorithm. This algorithm uses a weighted average of four estimates of the dependent variable over the interval Δt , to obtain the value at $t+\Delta t$.

$$\begin{aligned}
 k_1 &= f(x_0, t_0) \Delta t \\
 k_2 &= f(x_0 + k_1/2, t_0 + \Delta t/2) \Delta t \\
 k_3 &= f(x_0 + k_2/2, t_0 + \Delta t/2) \Delta t \\
 k_4 &= f(x_0 + k_3, t_0 + \Delta t) \Delta t \\
 x(t+\Delta t) &= (k_1 + 2k_2 + 2k_3 + k_4)/6 + x(t)
 \end{aligned} \tag{2.14}$$

The reliability and self-starting characteristics of this method were the motivating factors in the original selection of this algorithm. The choice of a suitable integration interval still remained. A trial and error procedure was employed to determine the appropriate step size. A series of simulations were examined, each with a successively larger step interval. When two consecutive simulations differed appreciably in their state histories, the next step interval tested was the average of the previous two values. This procedure resulted in the final choice of 0.1 seconds as the step interval. The ideal choice would have been an interval which satisfied the relation $\Delta t = 2^{-n}$, where n is an integer. Excessive computer execution time prevented the use of $\Delta t = 0.0625$ seconds ($n=4$); and $\Delta t = 0.125$ seconds ($n=3$) did not yield sufficient accuracy. With an interval of .10 seconds, the Runge-Kutta algorithm still consumed an undesirable amount of execution time. This

supplied the motivation to examine more rapid integration algorithms.

2.3.2) Milne-Reynold's Method

The method finally chosen was the Milne-Reynold's second order predictor-corrector algorithm [7]. This technique requires values of the dependent variables at the four previous discrete time points and is not self-starting. The Runge-Kutta algorithm is utilized for the first three time intervals to supply the three additional points. The Milne-Reynold's method is then used to complete the simulation.

The algorithm first estimates the derivative using the current ($t=t_0$) state variables. A predicted value of the state at $t=t_0+\Delta t$ is then obtained from the relation

$$p_{n+1} = x_{n-3} + \frac{4\Delta t}{3}(2f_n - f_{n-1} + 2f_{n-2}) \quad (2.15)$$

These predicted values, used in the system equations (2.7), (2.10), (2.11), (2.12), and (2.13), provide a revised estimate of the state variable derivatives.

$$\dot{p}_{n+1} = f(p_{n+1}, t_0 + \Delta t) \quad (2.16)$$

The corrected values for the state variables at $t_0 + \Delta t$ are then calculated.

$$x_{n+1} = (x_n + 7x_{n-1} + \frac{\Delta t}{24}(65\dot{p}_{n+1} + 243\dot{f}_n + 51\dot{f}_{n-1} + \dot{f}_{n-2}))/8 \quad (2.17)$$

The 0.10 second step interval was retained and a comparison of the Runge-Kutta and Milne-Reynold's methods was performed. Variations from the Runge-Kutta algorithm of 10^{-4} percent in displacement and 0.10 percent in the pitch rate were observed for a 300 second trajectory. Such a deviation is considered acceptable.

The reduction in the computer execution time was considerable. For each second of simulated time, the Runge-Kutta method required 1.07 seconds of execution time, the Milne-Reynold's method only 0.61 seconds. Thus, a 43 percent reduction in execution time was achieved by using the latter method.

2.4) Summary

The equations describing the aircraft's motion have been programmed. Initially a fourth order Runge-Kutta algorithm was considered as the integration method. However, the execution time proved excessive and a more suitable algorithm was sought. The algorithm finally chosen was the Milne-Reynold's predictor-corrector method. This method was chosen for its speed and stability characteristics. As a second order technique it required 43 percent less execution than did the Runge-Kutta. For every simulated second of flight the Milne-Reynold's method required 0.61 execution seconds.

3.0) Aircraft Model

3.1) Introduction

The nonlinear differential equations given in Chapter 2 are the general relationships governing the motion of an aircraft. The specific aircraft characteristics for a Boeing 737 are manifested in the dependence of the aerodynamic forces (X_S, Y_S, Z_S) and moments (L_S, M_S, N_S) on the vehicle state and control variables. An accurate model of these characteristics is necessary if the optimal trajectories are to be physically realized. In addition to the modeling of the aerodynamic data, the physical constraints on the aircraft must be faithfully reproduced. Constraints such as descent and ascent rates, maximum altitude, and speed restrict the set of trajectories from which the optimum can be determined. The following sections of this chapter detail the evolution of an appropriate aircraft model for a Boeing 737-100 utilizing two JT8D-7 turbofan engines.

3.2) Source of Data

Figure 3.1 illustrates the configuration of a Boeing 737-100 aircraft and includes the pertinent dimensions [5]. Aerodynamic data for this aircraft was obtained in the form of stability derivatives, supplied by the Flight Instrumen-

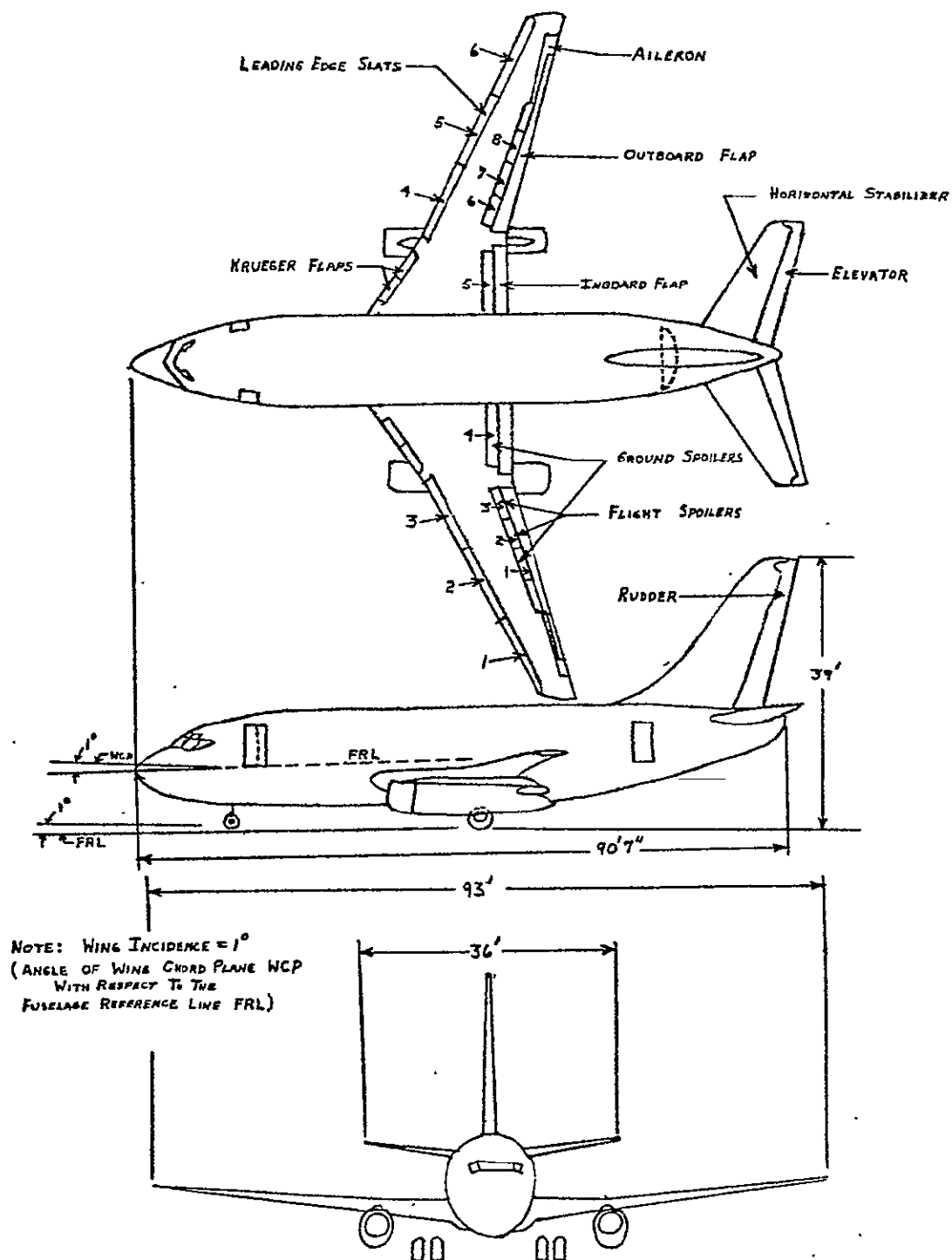


Figure 3.1

Boeing 737-100 Configuration

tation Division personnel at NASA's Langley Research Center. Figure 3.2 is a typical graph and illustrates the dependence of the basic lift coefficient on the angle of attack and the flap setting. The equations which define the total aerodynamic coefficients are presented in the Appendix.

3.3) Stability Derivative Simulation

The major task involved in developing the aircraft model was to adapt the aerodynamic data into a form more amenable to digital computation. The two alternate methods of adaptation considered were the direct storage of the graphical data and a functional approximation. Each has advantages and disadvantages which are described in the following sections.

3.3.1) Direct Data Storage

This method is a piecewise linear approximation of the data. For example, in Figure 3,2 each curve would be represented by data points chosen from that curve. The choice of the specific points depends upon the degree of nonlinearity. A second influential factor is the choice of either uniform or nonuniform abscissa intervals. The estimated computer storage requirement for uniform intervals is 3,000 decimal words. The abscissa intervals and ranges assumed in this estimate are given in Table I.

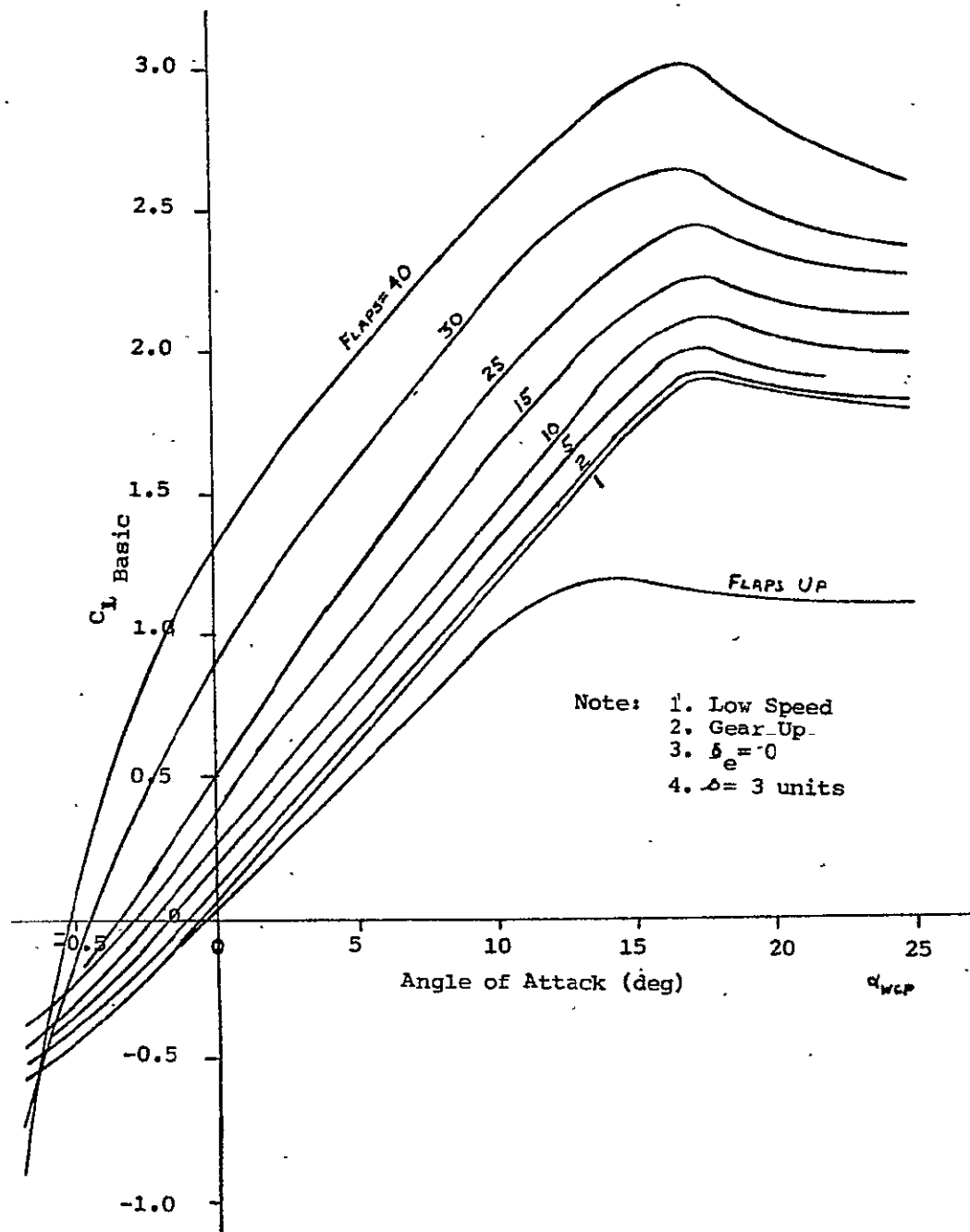


Figure 3.2
Basic Lift Coefficient

Table I
 Abscissa Uniform Interval Sizes and Ranges Used in
 the Direct Data Computer Storage Estimate

Abscissa Variable	Step Size	Total Range
Angle of Attack	3.0°	-5° to 5°
Mach Number	0.2	0 to 0.6
Rudder Deflection	5.0°	-25° to 25°
Aileron Deflection	10.0°	0° to 40°
Flight Spoiler Deflection	5.0°	0° to 40°
Sideslip Angle	5.0°	-15° to 15°

The use of nonuniform intervals required an estimated total of 1,600 data points. This estimate required fewer points per curve than the uniform interval method to achieve the same accuracy. However, a knowledge of both the ordinate and abscissa at each point was mandatory. The computer storage requirement was 3,200 decimal words. The logic needed for implementing either method was nearly equal. Therefore, if direct data storage were chosen as the adaptation technique, then uniform abscissa intervals would be more efficient.

3.2.2) Functional Approximation

The second alternative involved the identification of

functions which approximate the data to an acceptable degree of accuracy. A least-squares criterion was employed to generate the desired functions. A polynomial representation was chosen as the nominal function.

Figure 3.3 illustrates the comparison of two curves from Figure 3.2 and their respective polynomial approximations. These approximations are typical of the accuracy obtained and were judged as acceptable. The equations for the polynomials in Figure 3.3 are

$$\begin{aligned} C_{L_{Base}} = & 1.218 \times 10^{-3} + .1072 \alpha_{WCP} & (3.1a) \\ & + 3.266 \times 10^{-3} \alpha_{WCP}^2 - 5.247 \times 10^{-4} \alpha_{WCP}^3 \\ & + 1.173 \times 10^{-5} \alpha_{WCP}^4 \end{aligned}$$

for a flap setting of zero and

$$\begin{aligned} C_{L_{Base}} = & 1.216 + .1742 \alpha_{WCP} - 3.306 \times 10^{-3} \alpha_{WCP}^2 \\ & - 6.353 \times 10^{-5} \alpha_{WCP}^3 & (3.1b) \end{aligned}$$

for a flap setting of 40.

The computer program, which implemented the least-squares algorithm, fitted successively higher order polynomials to the data. The program terminated when the polynomial estimated the data points within an error of two percent.

Whenever possible, the coefficients of similar order polynomials were themselves fitted with least-squares polynomials in an effort to reduce the computer storage requirements. As an example, Figure 3.4 shows curves for each of five values of altitude (0, 13000, 20000, 23000,

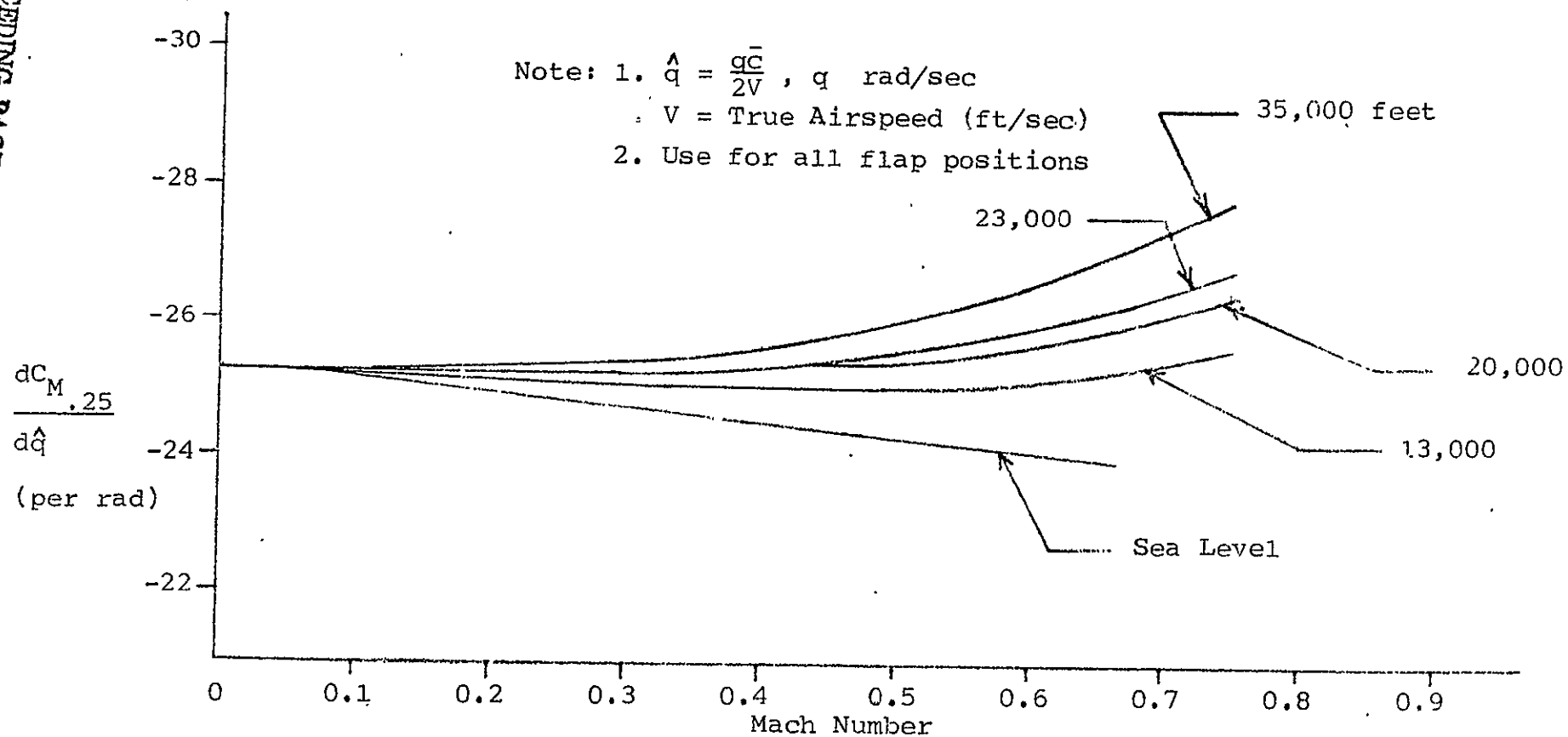


Figure 3.4
 Variation of the Pitching Moment Coefficient
 For Changes in the Pitch Rate

and 35000 feet). These curves were approximated by the polynomials

$$\left(\frac{dC_M}{d\hat{q}} \right)_{.25} \begin{cases} = 0.2533 - 0.02075 M; & h = 0 \text{ feet} \\ = 0.2519 - 0.00286 M; & h = 13000 \\ = 0.2522 - 0.00554 M; & h = 20000 \\ = 0.2518 + 0.00839 M; & h = 23000 \\ = 0.2508 + 0.01870 M; & h = 35000. \end{cases} \quad (3.2)$$

These equations have the form

$$Y = C_0 + C_1 M. \quad (3.3)$$

By treating each C_i as a function of the altitude, a least-squares approximation for each coefficient was obtained.

The result was that the five curves of Figure 3.4, which originally required the ten coefficients of equations (3.2), were represented by the single equation

$$\left(\frac{dC_M}{d\hat{q}} \right)_{.25} = (D_0 + D_1 h) + (D_2 + D_3 h + D_4 h^2) M; \quad (3.4)$$

$h = (0, 13000, 20000, 23000, 35000 \text{ feet})$

where

$$\begin{aligned} D_0 &= 0.2532 \\ D_1 &= -6.671 \times 10^{-8} \\ D_2 &= -2.078 \times 10^{-2} \\ D_3 &= 1.542 \times 10^{-6} \\ D_4 &= -1.177 \times 10^{-11}, \end{aligned}$$

and which contained only five coefficients.

For many stability derivatives the two percent error criterion required a polynomial of an undesirably high order.

For these derivatives piecewise polynomials of fourth order or less were used. Figure 3.5 shows a typical curve for which this method was applied. The polynomials and their applicable regions are

$$\left(\frac{dC_1}{d\beta}\right) \begin{cases} = -0.6582 + 8.796 \times 10^{-3} \alpha_{WCP} \\ \quad - 2.412 \times 10^{-3} \alpha_{WCP}^2 + 2.222 \times 10^{-4} \alpha_{WCP}^3 \\ \quad - 2.689 \times 10^{-6} \alpha_{WCP}^4; \quad (-5^\circ \leq \alpha_{WCP} \leq 20^\circ) \\ = -1.826 + 0.1458 \alpha_{WCP} - 2.973 \times 10^{-3} \alpha_{WCP}^2; \\ \quad (20^\circ \leq \alpha_{WCP} \leq 25^\circ). \end{cases} \quad (3.5)$$

In a further effort to reduce the number of coefficients, Fourier cosine series were fitted to the piecewise polynomials. These series approximations were originally used in twelve instances. The form of the series is

$$Y = C_0 + \sum_{k=1}^n C_k \cos\left[\left(\frac{2\pi kx}{T}\right) + \phi_k\right]. \quad (3.6)$$

If the series required fewer coefficients (C_k and ϕ_k) then the latter representation was used, otherwise the polynomials were retained. A second motivation to employ a Fourier series was the presence of roundoff errors. If the independent variable in a polynomial was the aircraft altitude, the difference between two nearly equal, large numbers was obscured by the roundoff errors.

Subsequent examination of the twelve Fourier series indicated that the accuracy of the approximation was not sufficient for seven of the derivatives. The piecewise-

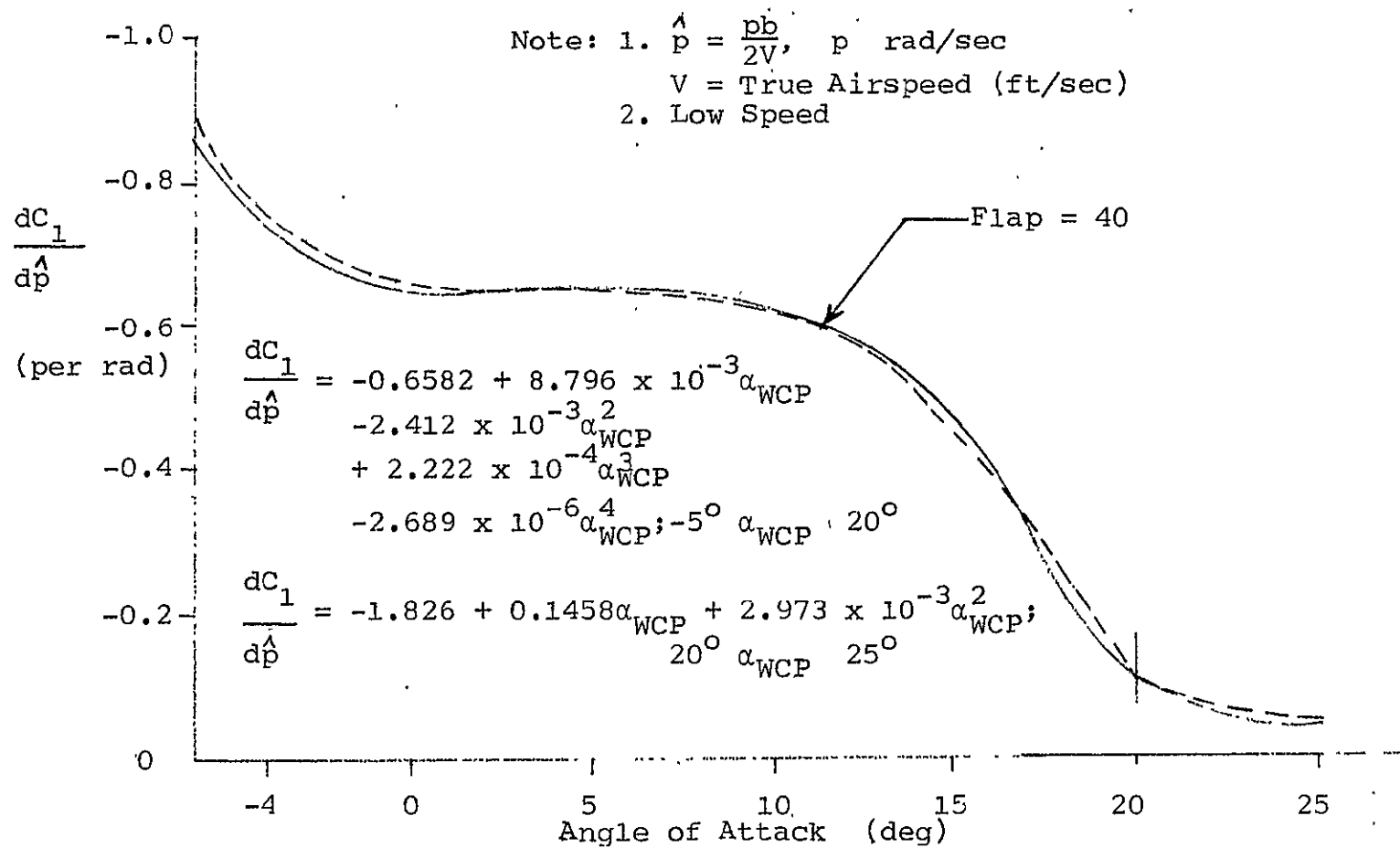


Figure 3.5
 Piecewise Fitted Polynomials

polynomials were reinstated for these stability derivatives. The functional approximation technique required 2,000 decimal words of computer storage.

3.3.3) Choice of Representation

The software logic complexity required for either direct data storage or functional approximation was estimated to be equal. Based upon the difference in the storage requirements of the two alternative methods, the functional approximation model was chosen. The effort to model all the stability derivatives by polynomials required an estimated 200 man-hours. An additional 200 man-hours were needed to develop an error-free software model. If computer storage is not a primary concern, considerable time could be saved by the use of direct data storage. The relatively short time to implement this data representation (20 to 40 Man-hours) greatly facilitates modification of the entire software package for an aircraft other than a Boeing 737-100.

3.3.4) Implementation

Returning to Figure 3.2, there are nine separate curves which describe the variation of the basic lift coefficient as the angle of attack changes. The choice of the appropriate curve is governed by the current setting of the

pilot flap quadrant located in the cockpit. This quadrant has nine discrete settings (0,1,2,5,10,15,25,30,40). Considerable programming complexity would have been required if the simulation permitted only these discrete flap settings. A decision was made to permit a continuous variation in flap setting in the range 0 to 40. The evaluation of any stability derivative at the intermediate flap settings is achieved by linear interpolation.

To illustrate the technique, assume the basic lift coefficient of Figure 3.2 is desired for an angle of attack of 5° and a flap setting of 32. First, the coefficient values for $\alpha_{WCP}=5^\circ$ and flaps at 30 and 40 are calculated to be 1.59 and 1.96, respectively. The value for a flap setting of 32 would then be interpolated to be 1.66. This same technique was employed for all curves having multiple parameter values. The variables used as parameters in modeling the aerodynamic data were flaps, rudder deflection, altitude, and angle of attack.

Special attention was directed to the modeling of the effectiveness factors for the flight spoilers and ailerons. The flight spoiler panels 2&3 ($k_{\delta sp1}$) can be deployed independent of panels 6&7 ($k_{\delta sp2}$). Therefore, separate values of $k_{\delta sp}$ must be calculated for each set of panels. Reference to Figures 3.1 and 3.6 indicate that both sets of spoilers produce negative lift and positive drag and pitch. Their contributions to the side force, roll and yaw moments require

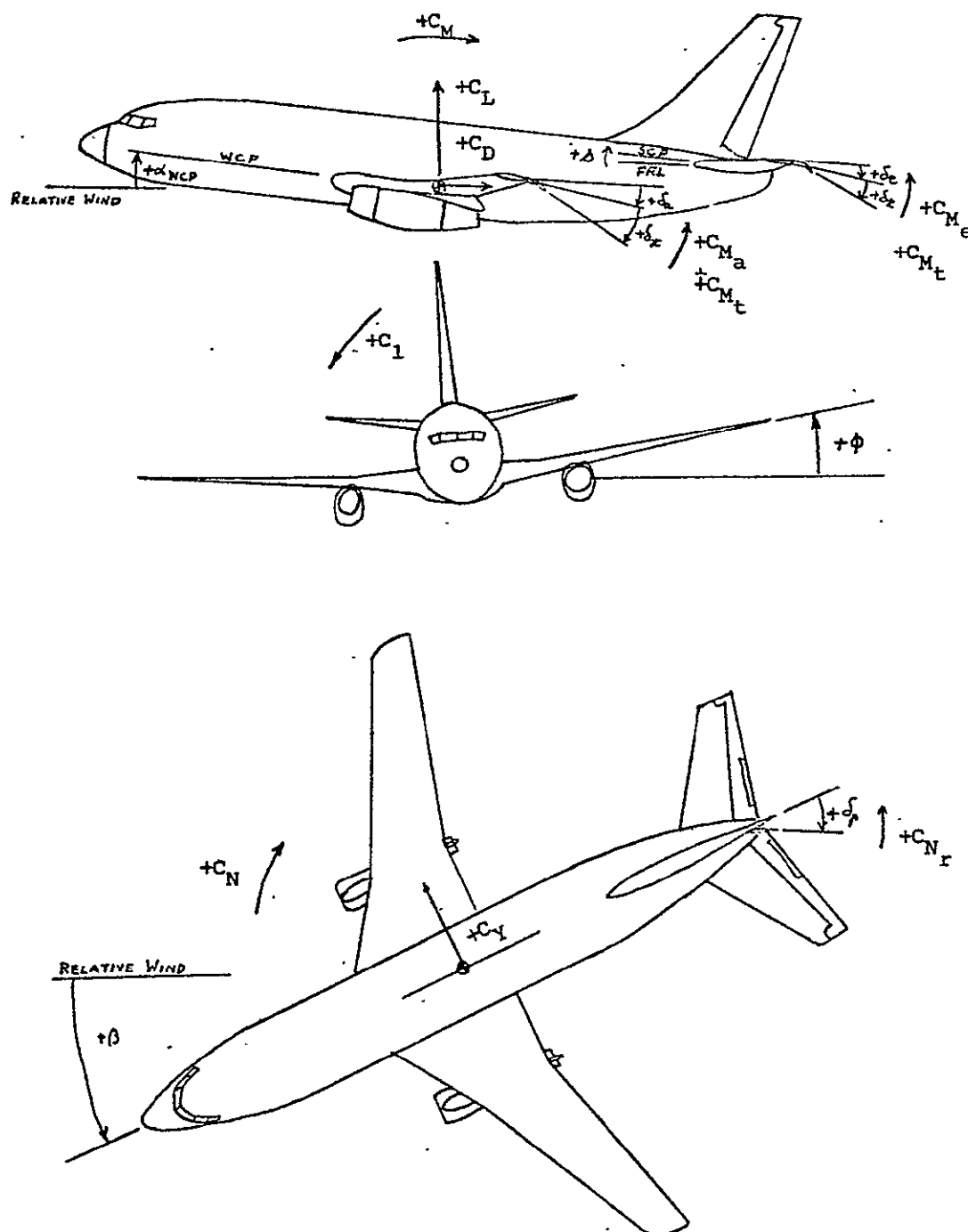


Figure 3.6

Aerodynamic Data Sign Convention

ORIGINAL PAGE IS
OF POOR QUALITY

$k_{\delta sp1} < 0$ and $k_{\delta sp2} > 0$. The ailerons are deployed symmetrically. A positive value for $k_{\delta a}$ (aileron effectiveness factor) occurs when the right aileron trailing edge is up.

3.4) Model Restrictions

A number of additional assumptions were made in the development of the aircraft model. Since the trajectories of interest are those of the landing phase only, the Mach number is not expected to exceed 0.6. Thus all stability derivatives dependent on the Mach number have been modeled only for speeds below a Mach number of 0.6. All trajectories should be examined to insure that the Mach number does not violate this assumption. If such a condition does occur, significant deviations from actual vehicle performance will result.

The ground effects in the aerodynamic data have been ignored. Thus the minimum "relative"¹ altitude for which the aircraft model is valid is 100 feet. Below this altitude ground effects become significant.

The ground spoilers on the aircraft were assumed to have been locked in the undeployed position. These controls are used only as speed brakes, when the aircraft is decelerating during the ground run phase of the landing maneuver.

¹"relative" altitude is defined as the height of the aircraft above the local ground plane.

The restriction on the minimum altitude eliminated the need to model these control surfaces.

Throughout the program the altitude is evaluated relative to the mean sea level. Thus the initial aircraft altitude for a trajectory is the sum of the airport altitude and the desired height of the vehicle above the local ground plane. The mean sea level altitude of any airport can be obtained from a document similar to [9].

The atmosphere used in the simulation is from [10]. The variation of the air density and speed of sound with altitude are described by (3.7).

$$\begin{aligned}\bar{\rho} &= 2.38 \times 10^{-3} (1 - 0.668 h)^{4.38} \\ a &= 1117 \exp(-0.36 \times 10^{-5} h)\end{aligned}\tag{3.7}$$

In addition, the atmosphere was assumed to have no wind velocity.

The aircraft total weight and moments of inertia were assumed constant over the entire trajectory. The effect of the constant weight assumption was tested in simulations restricted to the longitudinal plane. The variations in the aircraft performance are summarized in Table II. The largest deviation for a 180 second simulation does not exceed three percent. The moments of inertia were assumed constant for the tests. The variations were judged to be acceptable.

The fuel consumption of the JT8D-7 engine is, nominally,

Table II
Effect on Performance of The Constant
Weight and Moment of Inertia
Assumption

State Variable at $t_f = 180$ (s)	Variable Weight	Constant Weight	Variation (%)
Angle of Attack (deg)	3.7896	3.7801	0.25
Velocity (ft/sec)	209.02305	209.39176	-0.18
Pitch Rate (rad/sec)	-8.353×10^{-3}	-8.4375×10^{-3}	-1.01
Pitch Angle (deg)	1.01496	0.98450	3.00
X Ground Coordinate (ft)	-7206.167	-7199.2207	0.10
Y Ground Coordinate (ft)	29537.837	29505.158	0.11
Altitude (ft)	1686.0828	1675.8523	0.61

0.6 lbs/hr/lbf. For a thrust of 7,000 pounds, this is a fuel flowrate of 2.33 lbs/sec. If the total aircraft is 90,000 pounds and the trajectory duration is 500 seconds, the fuel consumed is 1.3 percent of the original weight. The added complexity of simulating the inertial time dependence was not considered justified for such a small increase in accuracy.

The landing gear was assumed locked in the deployed position during the entire trajectory. This assumption is not considered critical, since the contribution of the landing gear to the aerodynamic forces and moments is relatively small. In addition, the elevator was considered independent of the stabilizer. This was not strictly true and can be modified by specification of a control constraint.

A few of the stability derivatives were modeled in a special manner. For derivatives such as $(C_{nsp})_M / (C_{nsp})_{M=0}$, which have α_{WCP} as the parameter, the value for $\alpha_{WCP} < 0^\circ$ is evaluated assuming $\alpha_{WCP} = 0$. Similarly, when $\alpha_{WCP} > 6^\circ$ the stability derivative is calculated assuming $\alpha_{WCP} = 6^\circ$. Another derivative which required special consideration was $(dC_1/d\beta)$. This derivative is given for both high ($M > 0.4$) and low speeds. In an actual flight, the flaps are not deployed for high speeds. Under this condition $(dC_1/d\beta)$ has the Mach number as the parameter. For low speeds the parameter is flap setting. Due to the open loop nature of the control vector, it is possible for the flaps to be deployed when the

Mach number exceeds 0.4. When this occurs, the program evaluates the stability derivative as if the Mach number is less than 0.4. The use of penalty functions in the performance index can aid in removing these unrealistic conditions. Specifically, penalty functions which enforce the stall, buffet, and load factor constraints will heavily penalize the performance index whenever the flaps are deployed for Mach numbers in excess of 0.4. The optimization algorithm would then minimize the performance index by specifying a control history which would avoid these unrealistic conditions.

3.5) Aircraft State Constraints

If the simulation is to faithfully model the aircraft, the physical constraints on the vehicle must be enforced. This was accomplished by the addition of penalty functions (ψ_i) to the performance index. The various constraints and their respective penalty functions, which must be satisfied, are described in the paragraphs which follow.

3.51) Maximum Ascent and Descent Rates

The maximum rated ascent (descent) rate for the 737 is 100 (250) ft/sec. Whenever the glide slope is positive, the aircraft is climbing and the ascent rate is compared to the specified maximum. Therefore, the penalty functions have

the form

$$\begin{aligned}\psi_1 &= 10(\dot{h}/\text{Max. Asc. Rate}) \\ \psi_2 &= 0.\end{aligned}\tag{3.8}$$

Similarly, for negative glide slope the penalty functions are

$$\begin{aligned}\psi_1 &= 0 \\ \psi_2 &= 10(\dot{h}/\text{Max. Des. Rate}).\end{aligned}\tag{3.9}$$

The logic within the program has been designed to test \dot{h} and determine which of the forms (3.8) or (3.9) is to be used.

3.5.2) Altitude Constraints

As previously mentioned, the aerodynamic model ignores the ground effect which is negligible above a relative altitude of 100 feet. Thus, the minimum altitude (h_{\min}) for which aircraft performance can be accurately simulated is ($h_{\min} = h - h_{\text{airport}}$). The penalty function which enforces this condition is

$$\psi_3 = \left(\frac{h_{\min}}{h - h_{\text{airport}}} \right) 10.\tag{3.10}$$

The value h_{airport} is the mean sea level altitude of the airport and is specified in the program input data.

The maximum altitude (h_{\max}) depends upon the status of the flaps. If the flaps are not deployed, the limit is 35,000 feet; otherwise, it is 20,000 feet. The penalty

function has the form

$$\psi_4 = 10 \left(\frac{h}{h_{\max}} \right). \quad (3.11)$$

3.5.3) Load Factor

The structural limits of the aircraft must be enforced to prevent trajectories which require forces and moments that damage the vehicle. Typically, this constraint is displayed as the load factor limits shown in Figures 3.7 and 3.8. The load factor penalty for undeployed flaps is

$$\psi_5 = 10 \frac{|n_z - .75|}{1.75}. \quad (3.12)$$

Whenever the load factor is outside the region $-1 \leq n_z < 2.5$, the structural limit of the aircraft has been exceeded.

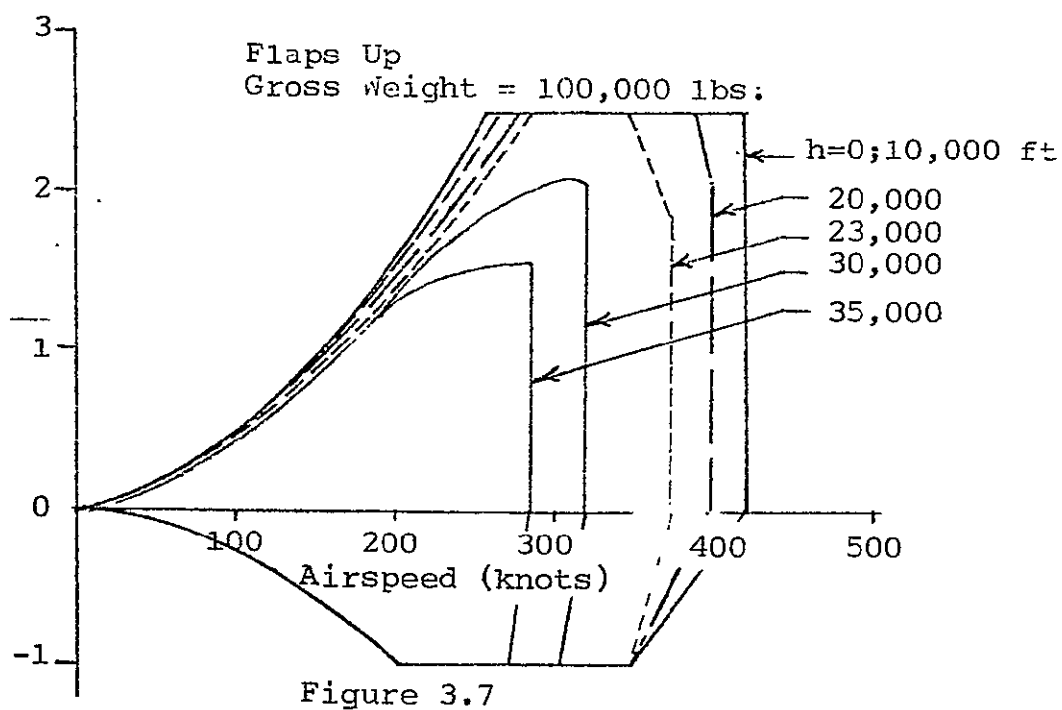
When the flaps are deployed the penalty is

$$\psi_5 = 10 |(n_z - 1.0)|. \quad (3.13)$$

3.5.4) Stall and Buffet

Figure 3.9 presents the stall speed characteristics of the aircraft. These curves are approximated by the linear functions

$$V_s \begin{cases} = 123.5 + 7.75 K; & \text{flaps} = 0 \\ = 99.25 + 6.75 K; & \text{flaps} = 1 \\ = 98.50 + 6.88 K; & \text{flaps} = 2 \end{cases} \quad (3.14a)$$



Load Factor Limit for Flaps Up

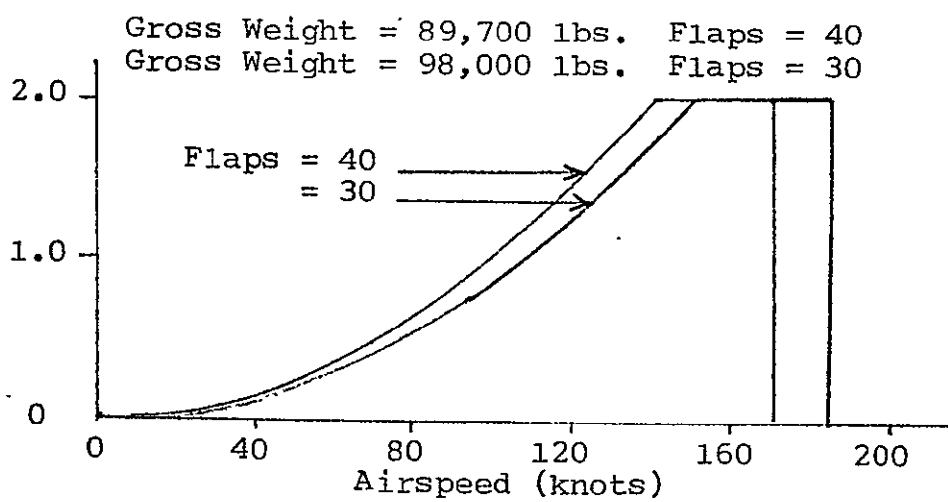


Figure 3.8

Load Factor Limit for Flaps Down

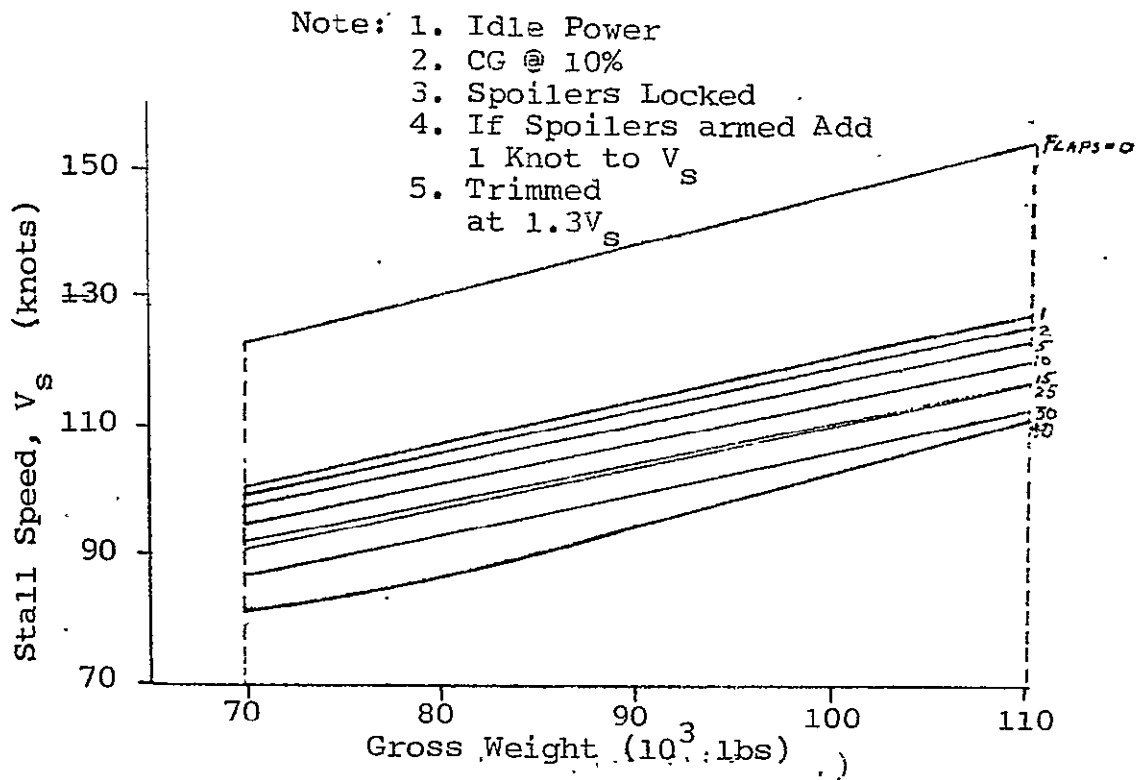


Figure 3.9

Stall Speed Characteristics

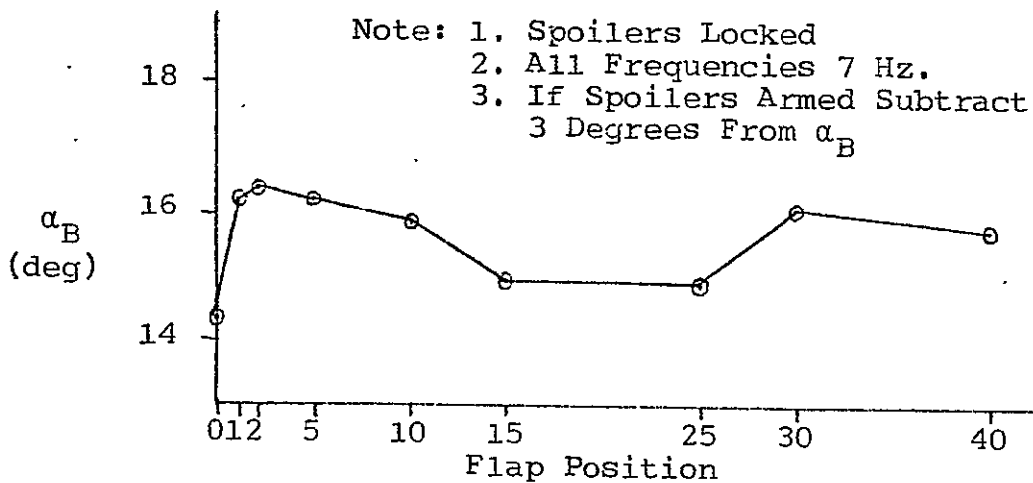


Figure 3.10

Low Speed Buffet Angle of Attack

$$\begin{array}{rcl}
 & = 97.00 + 6.63 K; & \text{flaps} = 5 \\
 \left. \begin{array}{l} \\ \\ \\ \\ \\ \end{array} \right\} V_s & \begin{array}{l} \\ \\ \\ \\ \\ \\ \end{array} & \begin{array}{l} \\ \\ \\ \\ \\ \\ \end{array} \\
 & = 94.00 + 6.38 K; & \text{flaps} = 10 \\
 & = 92.00 + 6.25 K; & \text{flaps} = 15 \\
 & = 90.50 + 6.50 K; & \text{flaps} = 25 \\
 & = 86.25 + 6.63 K; & \text{flaps} = 30 \\
 & = 80.00 + 7.60 K; & \text{flaps} = 45,
 \end{array} \quad (3.14b)$$

where V_s is the stall speed in knots, W is the aircraft gross weight in pounds, and

$$K = 10^{-4}(W - 70,000). \quad (3.14c)$$

The stall speed for intermediate flap settings is obtained by linear interpolation. These equations apply for undeployed flight spoilers. If the spoilers are deployed, an additional 1 knot is added to the value calculated from (3.14). The stall speed was assumed to be independent of both the center of gravity and the thrust level. The penalty function was developed to maintain a ten percent safety margin for V_s .

$$\psi_6 = 10\left(\frac{1.1 V_s}{V}\right) \quad (3.15)$$

This constraint is violated when the aircraft speed is lower than $1.1V_s$.

Figure 3.10 shows the low speed buffet angle of attack (α_B) as a function of the flap setting for undeployed spoilers. Linear interpolation between the discrete flap settings is used for intermediate values. The penalty function for low speed buffet is

$$\psi_7 = 10\left(\frac{\alpha_{WCP}}{\alpha_B}\right). \quad (3.16)$$

If the flight spoilers are deployed, then three degrees are subtracted from the calculated value of (α_B) . This modified value is then used in (3.16).

The high speed buffet constraint is shown in Figure 3.11 to be a limitation on the lift coefficient. This maximum lift coefficient (C_{Lp}) is approximated by a linear dependence on the Mach number of the form

$$C_{Lp} = 1.342 - 0.7122 M. \quad (3.17)$$

This relationship applies for Mach numbers above 0.24.

Below this value, (3.17) does not apply and C_{Lp} is set equal to zero ($\psi_8=0$). The penalty function for this constraint is

$$\psi_8 = 10\left(\frac{C_L}{C_{Lp}}\right), \quad (3.18)$$

where C_L is the current lift coefficient being tested.

3.5.5) Angle of Attack

An additional constraint on the angle of attack was formulated to insure the validity of the functions which represent the stability derivatives. A large proportion of the derivatives are functions of α_{WCP} . If this angle assumes values outside the range $(-5^\circ \leq \alpha_{WCP} \leq 25^\circ)$ the derivatives calculated would be grossly in error. To prevent this possibility the penalty function

$$\psi_9 = 10\left(\frac{\alpha_{WCP}^{-10}}{15}\right) \quad (3.19)$$

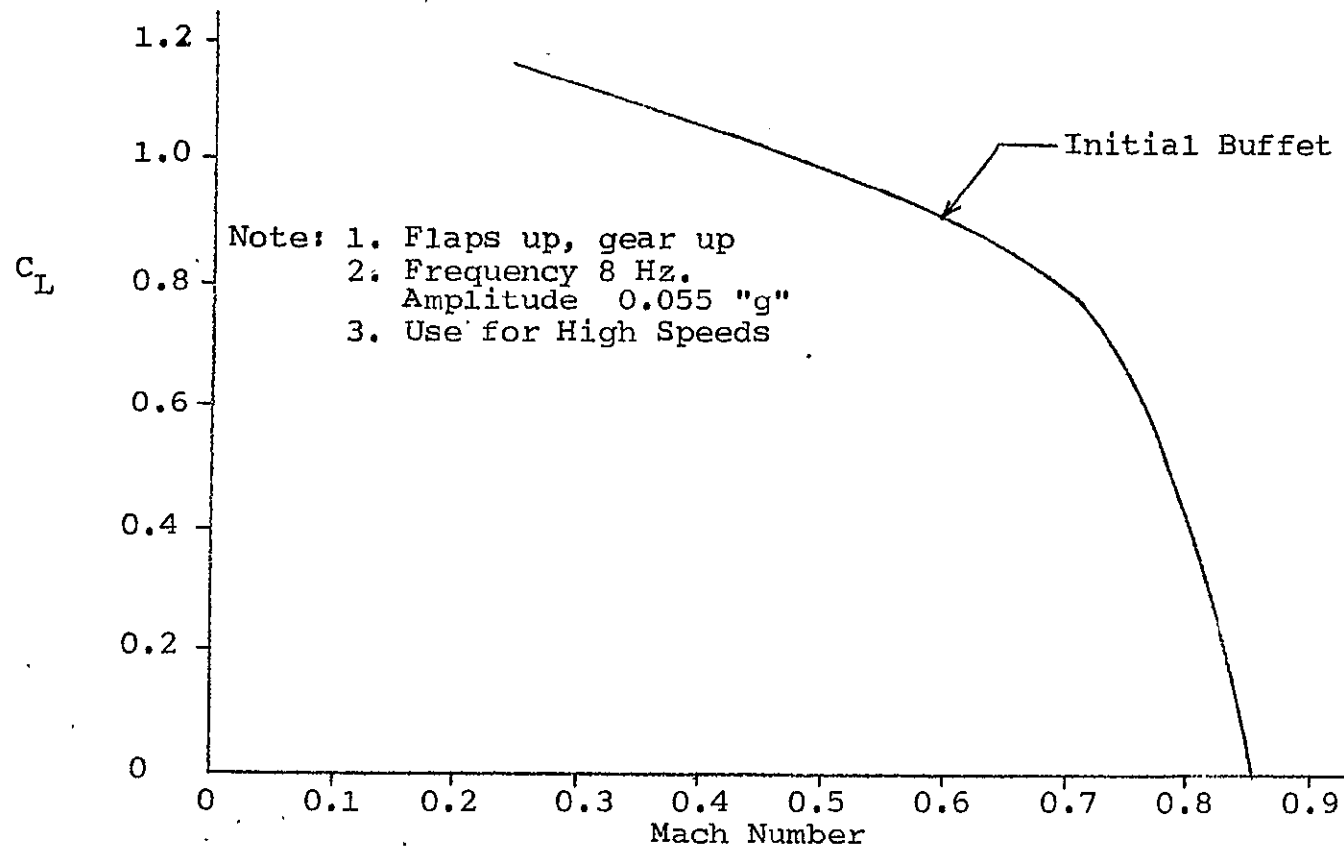


Figure 3.11
High Speed Buffet Lift Coefficient

is used.

3.6) Aircraft Control Surface Constraints

The aircraft control surfaces; i.e., elevator, rudder, etc., are subject to constraints which limit the vehicle's capability. These constraints are in the form of maximum displacements and displacement rates as described in this section. Table III presents the constraints for the various control surfaces under no load conditions. It was assumed that these rates also applied for loaded conditions.

Table III
Maximum Control Deflections and Actuation Rates

Control Surface	Maximum Displacement (deg)	Maximum Rate (deg/sec)
Elevator	± 21	± 56
Stabilizer	0-2.6	$\pm .56$
Manual Trim Wheel	0-17.0	± 3.27
Ailerons	± 20	± 66
(Panels 1,2,3,6,7,8) Spoilers	0-40.0	± 60
Rudder	± 24	± 56

The rate limit on the manual trim wheel cited in Table III is an estimated value. This estimate is based upon the assumption that the trim wheel displacement (s_p) is proportional to the stabilizer deflection (δ_s).

$$s_p = k \delta_s \quad (3.20)$$

The constant of proportionality, k , is assumed to be the ratio of the maximum displacements of the trim wheel to the stabilizer ($k = 17/2.6 = 6.54$). The trim wheel deflection rate is then obtained as the time derivative of (3.20) and noting that $\dot{\delta}_s = 0.50$ deg/sec in Table III.

The flap constraints have been modeled in a more complex manner. Table IV presents the flap displacement rate constraints. The operation times cited in the table are those times for which the flaps reached the particular position when started from an undeployed state at zero time.

The relative operation times in Table IV are considered constant; i.e., the time for the flaps to go from a position of 5 to 10 is the same as from 10 to 5, which is 4.37 seconds. It is important to realize that the simulated flap position reflects the current stabilizer deflection and not the actual pilot quadrant setting. The linkage system connecting the pilot quadrant to the stabilizer is assumed to have a negligible delay time.

The leading edges of the flaps have different operation times than those of Table IV. However, their contributions to the stability derivatives were not isolated in

Table IV
Flap Operation Times

Flap Position on Pilot Flap Quadrant	Normal Operation Time, (sec)
0	0.0
1	5.20
2	10.12
5	21.67
10	26.04
15	28.65
25	29.80
30	32.00
40	35.00

the data. Therefore, the assumption was made that all the flap aerodynamics were concentrated in the trailing edge. This allowed the leading edge operation times to be ignored.

The program logic was designed to test each control vector element to determine if the magnitude and rate constraints are satisfied. If the constraints are violated at a particular instant, the control value is adjusted to the constraint boundary value.

3.7) Aircraft Engine Constraints

Two Pratt & Whitney JT8D-7 turbofan engines are mounted on the wings and are symmetrically positioned relative to the aircraft vertical plane of symmetry. The characteristics of these engines are presented in this section.

3.7.1) Operational Limits

The range of thrust per engine was assumed to be 1,540 to 14,000 pounds. The simulation requires an accurate model of the engines because of the anticipated optimal trajectories. The optimization algorithm can be expected to generate flight paths which contain steep glide slopes. It is possible that the thrust requirements of an unconstrained

optimal trajectory will exceed the capability of the engines. Therefore, accurate models of the engine acceleration and deceleration characteristics are necessary.

Figure 3.12 displays the engine deceleration characteristics. The curves beginning at thrust levels below sixty percent of the maximum rated thrust were extrapolated from the original curves. The curve originating at the one hundred percent level has been approximated by

$$T' \begin{cases} = 1.0 - 0.95 t + 0.4125 t^2 - 0.0625 t^3; 0 \leq t \leq 3 \\ = 0.385 - 0.0925 t + 0.0075 t^2; 3 \leq t \leq 5 \\ = 0.11; t > 5, \end{cases} \quad (3.21)$$

where T' is the thrust per engine divided by 14,000 pounds.

For the eighty percent level

$$T' \begin{cases} = 0.80 - 0.70 t + 0.295 t^2 - 0.0442 t^3; 0 \leq t \leq 3 \\ = 0.325 - 0.07 t + 0.005 t^2; 3 \leq t \leq 5 \\ = 0.11; t > 5, \end{cases} \quad (3.22)$$

for the sixty percent level

$$T' \begin{cases} = 0.60 - 0.4517 t + 0.1775 t^2 - 0.0258 t^3; 0 \leq t \leq 3 \\ = 0.253 - 0.0405 t + 0.0015 t^2; 3 \leq t \leq 5 \\ = 0.11; t > 5, \end{cases} \quad (3.23)$$

for the forty percent level

$$T' \begin{cases} = 0.40 - 0.1125 t - 0.015 t^2 + 0.0075 t^3; 0 \leq t \leq 3 \\ = 0.22 - 0.03t; 3 \leq t \leq 4 \\ = 0.11; t > 4, \end{cases} \quad (3.24)$$

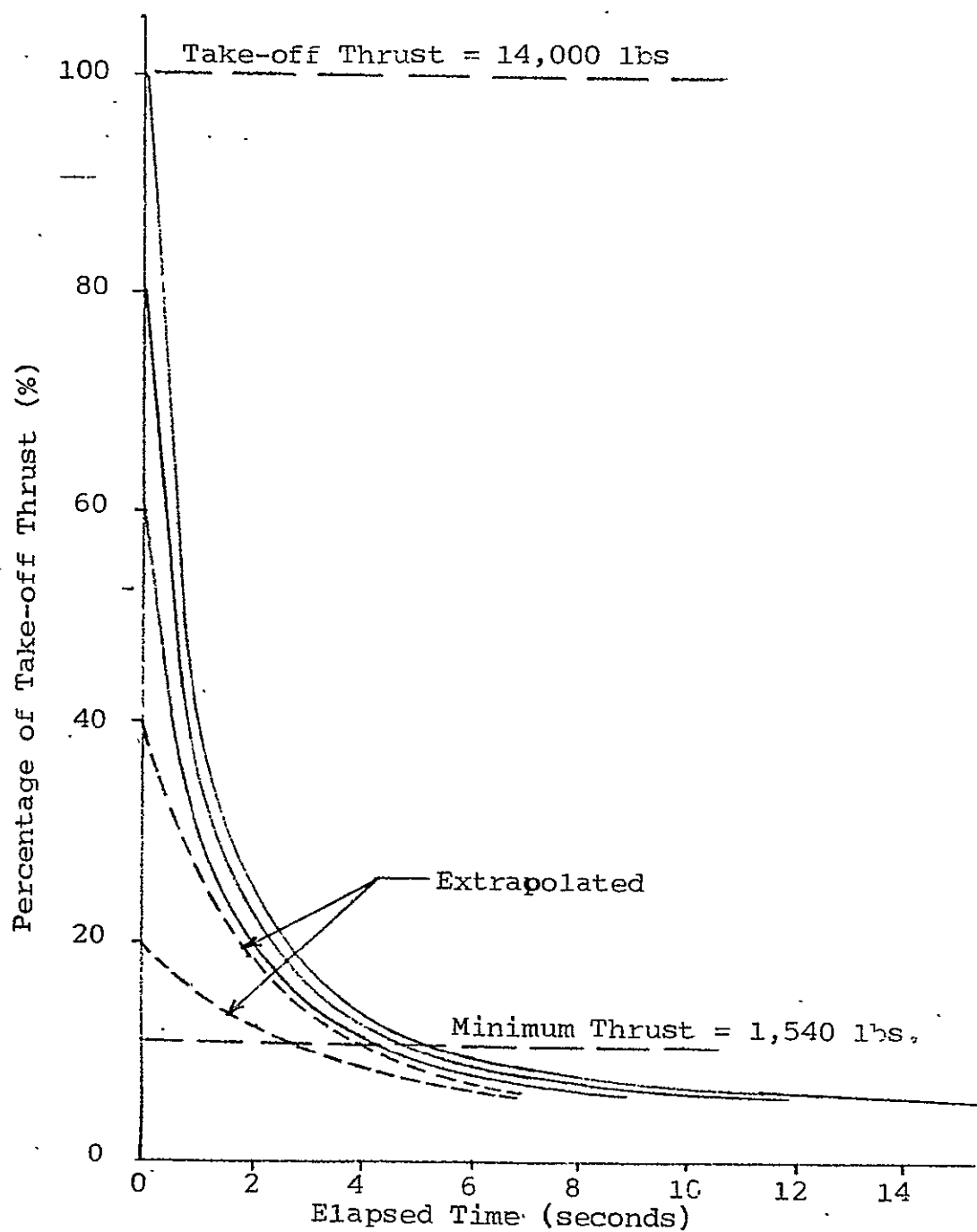


Figure 3.12
Engine Deceleration Characteristics

for the twenty percent level

$$T' \begin{cases} = 0.20 - 0.0633 t + 0.015 t^2 - 0.001667 t^3; 0 \leq t \leq 2.6 \\ = 0.11; t > 2.6, \end{cases} \quad (3.25)$$

and for thrust levels below twenty percent

$$T' \begin{cases} = \bar{T} - 0.0633 t + 0.015 t^2 - 0.001667 t^3; 0 \leq t \leq 2.6 \\ = 0.11; t > 2.6 \end{cases} \quad (3.26)$$

where \bar{T} is the thrust level coinciding with the initiation of the engine deceleration sequence.

The program logic was constructed to identify the thrust level at the initiation of an engine deceleration interval. The thrust constraints for subsequent deceleration times are calculated using linear interpolation. The actual thrust level at each time is compared to the constraint magnitude. If the constraint is violated, the thrust is adjusted to that value of the constraint; otherwise it is left unchanged. In this manner the simulated thrust history is assured to have realistic deceleration characteristics.

The engine acceleration curves are shown in Figure 3.13. The functional approximation of the curves originating at the ten percent level is

$$T' \begin{cases} = 0.10 + \frac{1}{150} t; 0 \leq t \leq 1.5 \\ = 0.11 + \frac{t-1.5}{7.714}; 1.5 \leq t \leq 2.85 \\ = 0.285 + (t - 2.85) 0.38; t > 2.85, \end{cases} \quad (3.26)$$

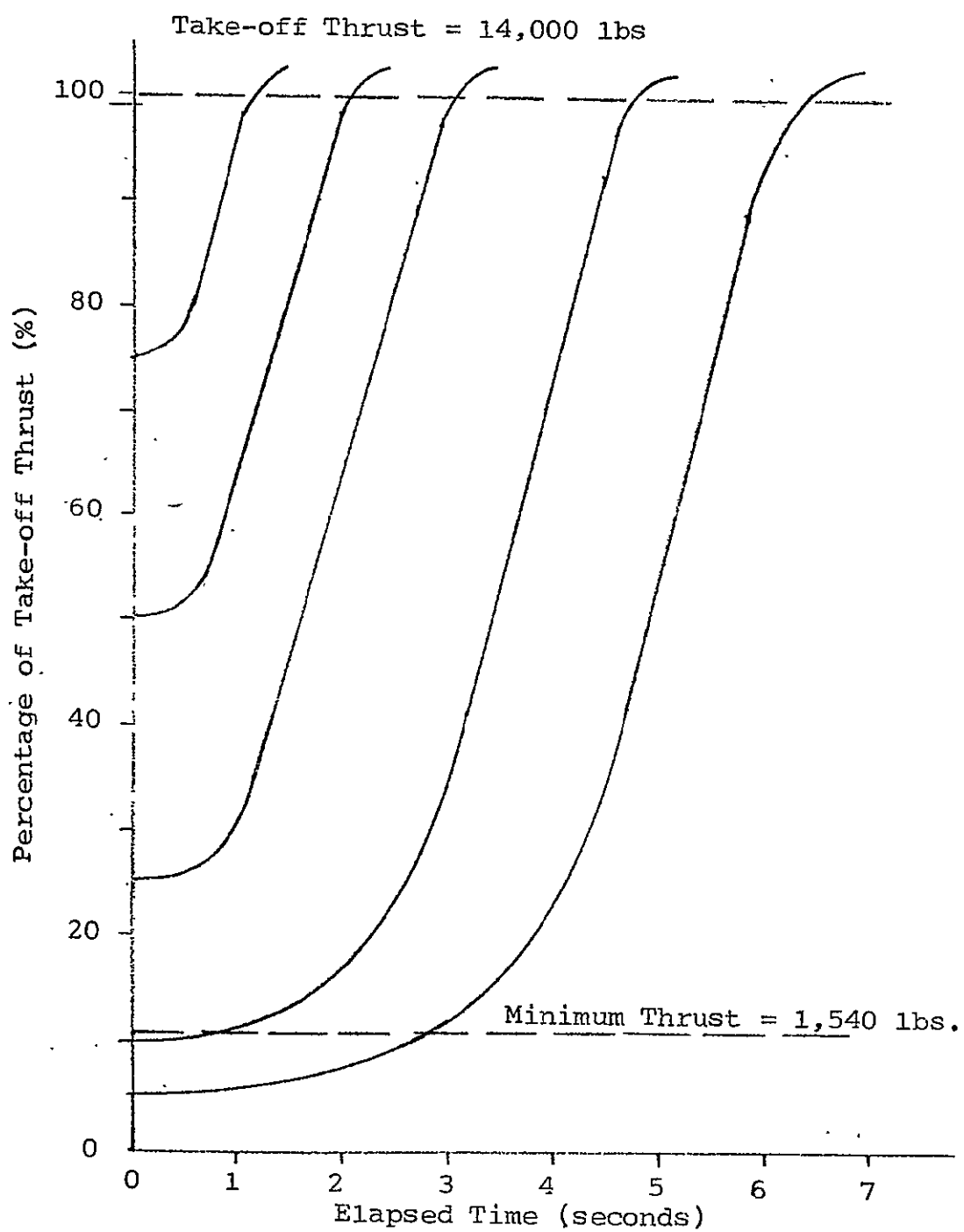


Figure 3.13

Engine Acceleration Characteristics

for the twenty-five percent level

$$T' \begin{cases} = 0.25 + 0.01 t; 0 \leq t \leq 1.0 \\ = 0.26 + 0.38(t-1.0); t > 1.0, \end{cases} \quad (3.27)$$

for the fifty percent level

$$T' \begin{cases} = 0.50 + \frac{1}{65.0} t; 0 \leq t \leq 0.65 \\ = 0.51 + 0.38(t-0.65); t > 0.65, \end{cases} \quad (3.28)$$

for the seventy-five percent level

$$T' \begin{cases} = 0.75 + \frac{1}{45.0} t; 0 \leq t \leq 0.45 \\ = 0.76 + 0.38(t-0.45); t > 0.45, \end{cases} \quad (3.29)$$

for an initial thrust \bar{T} above the seventy-five percent level

$$T' = \bar{T} + 0.38 t; t > 0. \quad (3.30)$$

The thrust levels during an engine acceleration sequence are determined by the same method used for the deceleration case. In this manner a realistic simulation of the engine acceleration characteristics is achieved.

3.7.2) Fuel Consumption Model

The performance index contains a component which represents the fuel consumed during a simulation. The performance index was formulated to permit arbitrary weighting of the various components (time, fuel, and noise). If the fuel consumption is a significant component an accurate model of the flowrate is necessary. Thrust specific fuel

consumption (TSFC) data, obtained from NASA Langley personnel, are shown in Figures 3.14 through 3.16. [10]. The data displays the dependence of TSFC on Mach number, thrust, and altitude. These curves are strictly valid for the altitudes (10,000; 5,000; 0). For altitudes above 10,000 feet the TSFC curves for the latter altitude were used. If the Mach number exceeds 0.6, the 0.6 Mach number data are used.

For a given altitude and Mach number, the TSFC, having dimensions of lbs/hr/lbf, was obtained as a function of the thrust using a least-squares polynomial criterion. For each discrete Mach number (0.0, 0.1, 0.2, 0.3, 0.4, 0.5, 0.6) and altitude (0, 5000, 10000 feet), a separate function is used. The approximation polynomials at sea level are

$$\text{TSFC} \left\{ \begin{array}{l}
 = 1.244 - 0.3167 F + 0.0545 F^2 - 4.0 \times 10^{-3} F^3 \\
 \quad + 1.08 \times 10^{-4} F^4; M=0.0, 0.1 \\
 = 1.390 - 0.3534 F + 0.0599 F^2 - 4.385 \times 10^{-3} F^3 \\
 \quad + 1.18 \times 10^{-4} F^4; M=0.2 \\
 = 1.704 - 0.4973 F + 0.0884 F^2 - 6.765 \times 10^{-3} F^3 \\
 \quad + 1.88 \times 10^{-4} F^4; M=0.3 \\
 = 1.896 - 0.5534 F + 0.0964 F^2 - 7.25 \times 10^{-3} F^3 \\
 \quad + 1.99 \times 10^{-4} F^4; M=0.4 \\
 = 2.653 - 1.137 F + 0.2784 F^2 - 0.0334 F^3 \\
 \quad + 1.933 \times 10^{-3} F^4 - 4.306 \times 10^{-5} F^5; M=0.5 \\
 = 4.58 - 2.76 F + 0.56 F^2; M=0.6, F \leq 2.5 \\
 = 1.949 - 0.4641 F + 0.0729 F^2 - 5.109 \times 10^{-3} F^3 \\
 \quad + 1.334 \times 10^{-4} F^4; M=0.6, F > 2.5,
 \end{array} \right. \quad (3.31)$$

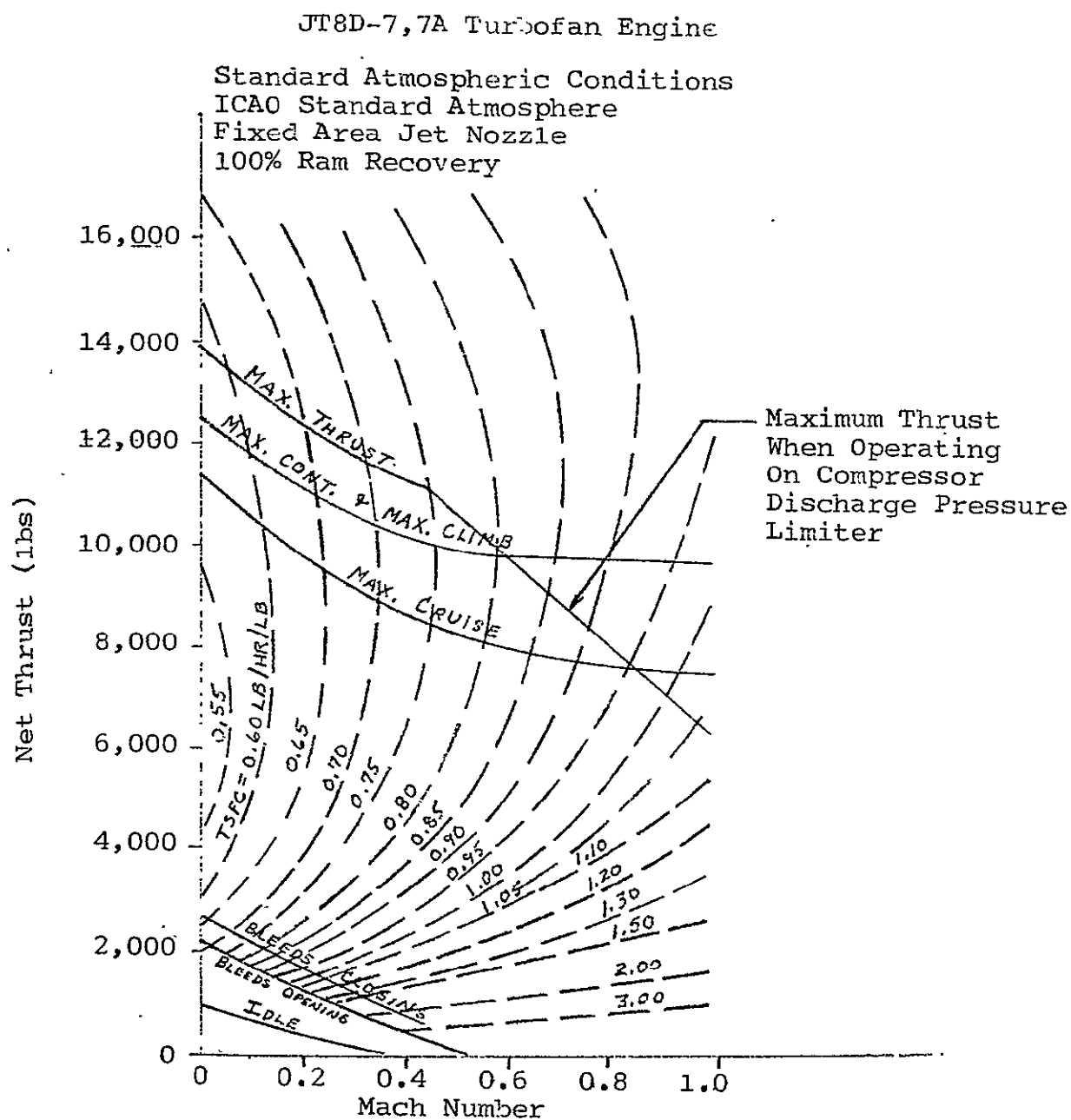


Figure 3.14

Thrust Specific Fuel Consumption at Sea Level

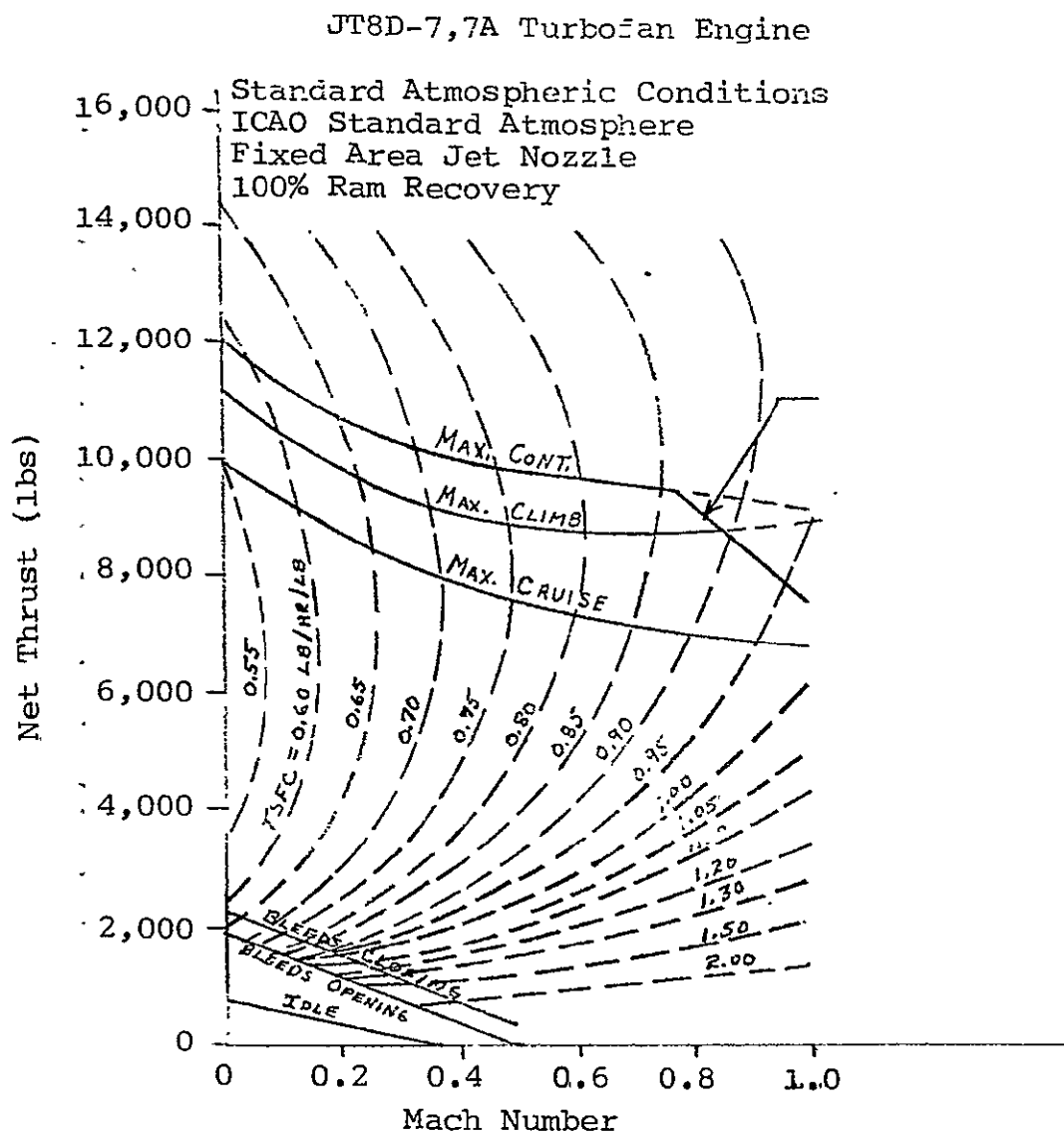


Figure 3.15

Thrust Specific Fuel Consumption at 5,000 Feet

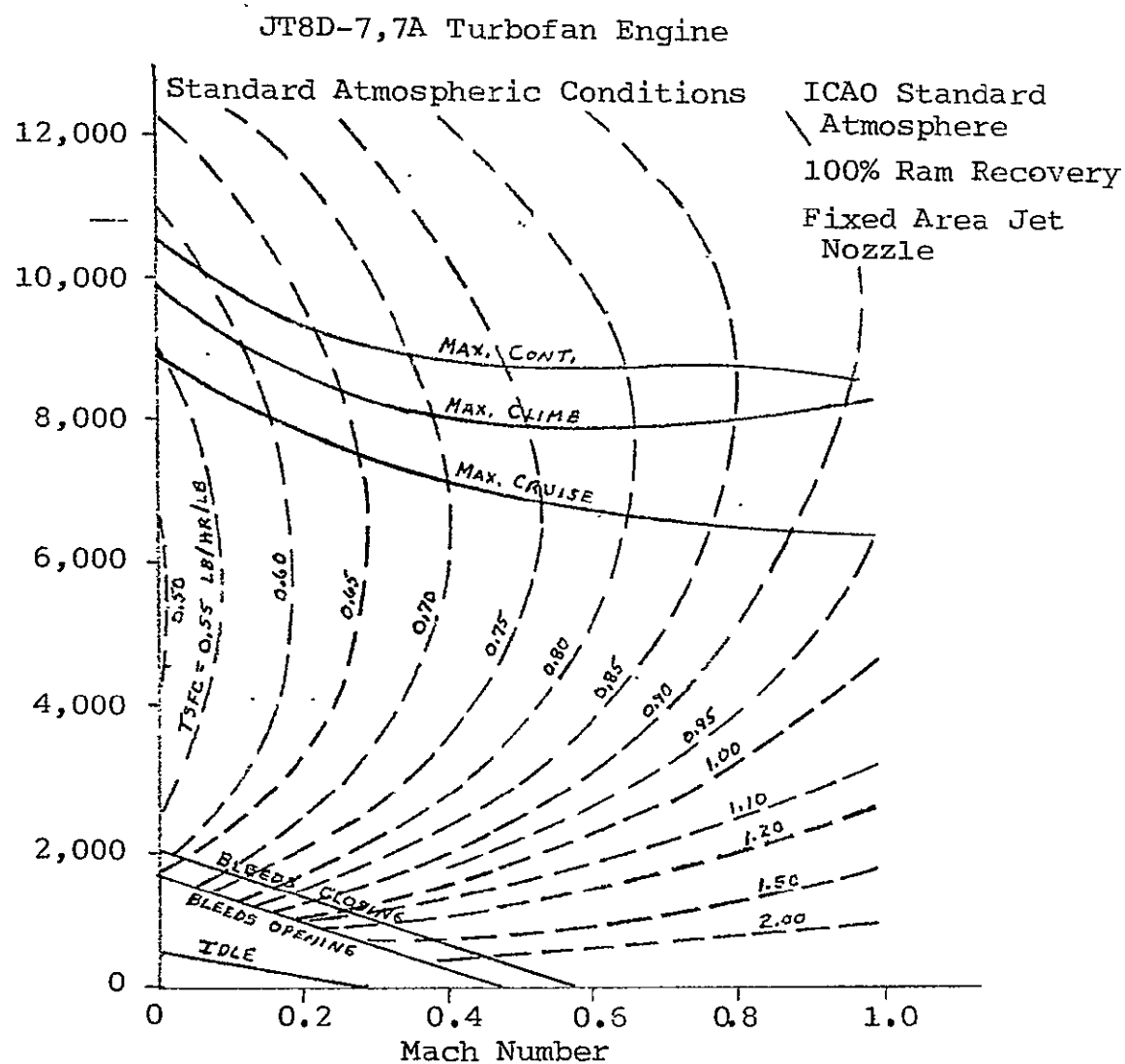


Figure 3.15

Thrust Specific Fuel Consumption at 10,000 Feet

where F is the thrust of one engine divided by 1,000 pounds. The approximation polynomials for an altitude of 5,000 feet are

$$\begin{aligned}
 \text{TSFC} \left\{ \begin{aligned}
 &= 1.133 - 0.29 F + 0.0527 F^2 - 4.05 \times 10^{-3} F^3 \\
 &\quad + 1.144 F^4; M=0.0, 0.1 \\
 &= 1.353 - 0.3769 F + 0.0685 F^2 - 5.267 \times 10^{-3} F^3 \\
 &\quad + 1.48 \times 10^{-4} F^4; M=0.2 \\
 &= 1.453 - 0.3855 F + 0.0678 F^2 - 5.11 \times 10^{-3} F^3 \\
 &\quad + 1.42 \times 10^{-4} F^4; M=0.3 \quad (3.32) \\
 &= 1.568 - 0.3989 F + 0.06728 F^2 - 4.89 \times 10^{-3} F^3 \\
 &\quad + 1.32 \times 10^{-4} F^4; M=0.4 \\
 &= 2.174 - 0.8681 F + 0.2147 F^2 - 0.0261 F^3 \\
 &\quad + 1.54 \times 10^{-3} F^4 - 3.489 \times 10^{-5} F^5; M=0.5 \\
 &= 3.83 - 1.32 F; M=0.6, F \leq 2.0 \\
 &= 1.774 - 0.4202 F + 0.06649 F^2 - 4.61 \times 10^{-3} F^3 \\
 &\quad + 1.19 \times 10^{-4} F^4; M=0.6, F > 2.0,
 \end{aligned} \right.
 \end{aligned}$$

and an altitude of 10,000 feet are

$$\begin{aligned}
 \text{TSFC} \left\{ \begin{aligned}
 &= 1.062 - 0.2934 F + 0.06 F^2 - 5.19 \times 10^{-3} F^3 \\
 &\quad + 1.674 \times 10^{-4} F^4; M=0.0, 0.1 \\
 &= 1.2329 - 0.3578 F + 0.0729 F^2 - 6.356 \times 10^{-3} F^3 \\
 &\quad + 2.06 \times 10^{-4} F^4; M=0.2 \quad (3.33) \\
 &= 1.2398 - 0.3038 F + 0.0569 F^2 - 4.623 \times 10^{-3} F^3 \\
 &\quad + 1.428 \times 10^{-4} F^4; M=0.3 \\
 &= 1.433 - 0.3868 F + 0.07376 F^2 - 6.08 \times 10^{-3} F^3 \\
 &\quad + 1.88 \times 10^{-4} F^4; M=0.4 \\
 &= 1.575 - 0.4271 F + 0.0793 F^2 - 6.38 \times 10^{-3} F^3 \\
 &\quad + 1.92 \times 10^{-4} F^4; M=0.5
 \end{aligned} \right.
 \end{aligned}$$

$$\text{TSFC} = 1.7095 - 0.4778 F + 0.09 F^2 - 7.376 \times 10^{-3} F^3 + 2.24 \times 10^{-4} F^4; M=0.6.$$

The TSFC is converted into fuel flowrate (lbs/sec) by the relationship

$$\dot{m} = \text{TSFC} (2 \text{ engines}) (\text{Thrust/engine}) / (3,600 \text{ sec/hr}) \quad (3.34)$$

Interpolation is used for Mach numbers and altitude other than those for which (3.31) through (3.33) apply. As an example, assume the value for TSFC is desired at a Mach number of 0.45, an altitude of 3,000 feet, and a thrust of 4,000 pounds. First the values of TSFC at sea level, for Mach numbers of 0.4 and 0.5 are calculated to be 0.811 and 0.873, respectively. The interpolated value at a Mach number of 0.45 and sea level altitude is 0.842. Similarly, the interpolated value at 5,000 feet is 0.784. Interpolating for the altitude of 3,000 feet and a Mach number of 0.45 gives 0.807. In terms of the fuel flowrate, this is 1.79 lbs/sec.

This model could be considered too complex for some applications of the optimization program. Specifically, when the fuel component of the performance index is relatively small, the model is inefficient. However, the relative sizes of the components are determined by the program user, and the more accurate model presented above is necessary.

3.8) Model Accuracy

The previous sections have detailed the development of a software model for a Boeing 737 aircraft. The foundation upon which the model has been built is the least-squares polynomial approximation of the stability derivatives. If this representation of the aerodynamic data does not realistically simulate the aircraft performance, then the generated optimal trajectories are meaningless. Therefore, considerable effort was expended to verify the model's accuracy.

Four cases have been chosen to evaluate the model accuracy. Case #1 is the aircraft state at one instant along a -3 degree glide slope confined to the vertical plane. Case #2 is from a -6 degree glide slope which was also restricted to only longitudinal motion. Case #3 is from a more general trajectory confined to longitudinal motion. Finally, Case #4 is from a 20 degree banked turn. The aircraft state and properties for each of the cases are summarized in Table V.

Table VI is a comparison of the lift coefficients of the model with a manual estimate obtained from the original data given in [5]. The results for each of the four cases demonstrate an excellent correspondence between the model and the actual values for the total lift coefficients.

ORIGINAL PAGE IS
OF POOR QUALITY

PRECEDING PAGE BLANK NOT FILMED

Table VI

Comparison of the Lift Coefficients
of the Model and the Original Data

	CASE #1			CASE #2			CASE #3			CASE #4		
COEFFICIENT COMPONENT	ORIG. DATA	MODEL	Δ (%)	ORIG. DATA	MODEL	Δ (%)	ORIG. DATA	MODEL	Δ (%)	ORIG. DATA	MODEL	Δ (%)
$C_{L \text{ BASIC}}$	1.960	1.977	1.9	1.970	2.013	2.2	1.950	1.964	0.7	2.150	2.191	1.9
$\Delta \frac{\partial C_L}{\partial \alpha}^* \alpha_{WCP} (10^3)$	-7.50	-4.624	38.3	-7.680	-4.735	38.3	-7.170	-4.365	38.9	-9.748	-5.998	38.5
$\frac{\partial C_L}{\partial \delta} \hat{\delta} (10^4)$	-4.436	-4.423	0.3	-4.436	-4.427	0.3	-4.436	-4.423	0.3	-4.436	-4.421	0.3
$\frac{\partial C_L}{\partial \delta} \hat{\delta} (10^4)$	4.551	4.492	1.3	3.898	3.826	1.8	3.898	3.829	1.8	4.551	4.486	1.4
$\frac{\partial C_L}{\partial \alpha} \alpha (10^3)$	7.505	7.535	0.4	7.110	7.138	0.4	7.90	7.934	0.4	7.90	7.907	0.1
$\Delta C_{L \Delta p} (10^3)$	-5.651	-5.692	0.7	-6.787	-6.825	0.6	-4.904	-4.383	0.5	-10.03	-9.539	4.9
$\Delta C_{L \delta_c} (10^3)$	2.454	2.485	1.3	2.283	2.308	1.1	2.648	2.653	0.2	1.708	1.642	3.8
$(C_{L_0})_M - (C_{L_0})_{M=0}$	0	0	0	0	0	0	0	0	0	0	0	0
$\Delta C_{L \Delta p} (10^3)$	-5.60	-5.572	0.5	-5.60	-5.521	1.3	-5.50	-5.544	0.8	-5.90	-5.612	4.8
$C_{L \text{ TOTAL}}$	1.872	1.912	2.1	1.868	1.914	2.5	1.878	1.895	0.9	2.006	2.058	2.6

$$* \Delta \frac{\partial C_L}{\partial \alpha} \alpha_{WCP} = \left[\left(\frac{\partial C_L}{\partial \alpha} \right)_M - \left(\frac{\partial C_L}{\partial \alpha} \right)_{M=0} \right] \alpha_{WCP}$$

Examining the component due to α_{WCP} indicates a large error in the model's representation of $(dC_L/d\alpha)$. However, the relatively small contribution which this component has toward the total value limits the effect of the error to an acceptable level.

Tables VII and VIII compare the model and original data for the drag and lateral force coefficients, respectively. The drag coefficient in the model has a large error for the sideslip component. The sideslip contributes approximately 0.03 percent of the total drag coefficient in case #4, and a large error in representing this component is unimportant. The lateral force coefficient has all of its components accurately modeled. Therefore, the aerodynamic forces (lift, drag, and lateral) can be assumed to be accurately represented by the model.

Tables IX, X, and XI show the comparison for the pitch, roll, and yaw moment coefficients, respectively. The worst aggregate error in the pitch model occurs for case #4. The 13.3 percent error is marginally acceptable. Currently this error will be tolerated, but if future circumstances warrant it, the model accuracy can be improved. The roll moment coefficient also has a large aggregate model error. However closer examination of Table X indicates that a near equilibrium condition of zero roll occurs. The absolute value of the 156 percent error can be estimated to cause

Table VII
Comparison of the Drag Coefficients
of the Model and the Original Data

COEFFICIENT COMPONENT	CASE #1			CASE #2			CASE #3			CASE #4		
	ORIG. DATA	MODEL	Δ (%)	ORIG. DATA	MODEL	Δ (%)	ORIG. DATA	MODEL	Δ (%)	ORIG. DATA	MODEL	Δ (%)
$C_{D \text{ BASIC}}$	0.2660	0.2638	0.8	0.2680	0.2656	0.9	0.2640	0.2599	1.6	0.2910	0.2880	1.0
$\Delta C_{D \text{ GEAR}} (x 10^2)$	0.790	0.804	1.8	0.770	0.7760	3.1	0.810	0.8258	1.9	0.670	0.6885	2.8
$\Delta C_{D \text{ SIDESLIP}} (x 10^2)$	0	0	0	0	0	0	0	0	0	-1.0	-1.6367	36.0
$\Delta C_{D \text{ RUDDER}} (x 10^2)$	0	0	0	0	0	0	0	0	0	0.10	0.262	162.
$C_{D \text{ TOTAL}}$.2739	.2718	0.8	.2757	.2736	0.8	.2721	.2681	1.5	.2986	.2977	0.4

Table VIII
Comparison of the Lateral Coefficients
of the Model and the Original Data

	CASE #1			CASE #2			CASE #3			CASE #4		
COEFFICIENT COMPONENT	ORIG. DATA	MODEL	Δ (%)	ORIG. DATA	MODEL	Δ (%)	ORIG. DATA	MODEL	Δ (%)	ORIG. DATA	MODEL	Δ (%)
$\frac{\partial C_Y}{\partial \beta} \beta \text{ (x10}^4\text{)}$	0	0	0	0	0	0	0	0	0	.1226	.1218	0.7
$\frac{\partial C_Y}{\partial \beta} \beta \text{ (x10}^4\text{)}$	0	0	0	0	0	0	0	0	0	.2854	.2852	.09
$\frac{\partial C_Y}{\partial \beta} \beta \text{ (x10}^4\text{)}$	0	0	0	0	0	0	0	0	0	.0920	.1039	12.9
$\Delta C_{Y_{AILERON}} \text{ (x10}^5\text{)}$	0	0	0	0	0	0	0	0	0	~0	-.1502	—
$\Delta C_{Y_{RUDDER}} \text{ (x10}^4\text{)}$	0	0	0	0	0	0	0	0	0	-.1632	-.1616	1.0
$C_{Y_{TOTAL}} \text{ (x10}^5\text{)}$	0	0	0	0	0	0	0	0	0	-.4023	-.3948	1.9

Table IX

Comparison of the Pitch Coefficients
of the Model and the Original Data

	CASE #1			CASE #2			CASE #3			CASE #4		
COEFFICIENT COMPONENT	ORIG. DATA	MODEL	Δ (%)	ORIG. DATA	MODEL	Δ (%)	ORIG. DATA	MODEL	Δ (%)	ORIG. DATA	MODEL	Δ (%)
$C_{M,25,BASIC}$	-1.2870	-1.2864	0.2	-1.2870	-1.2892	0.8	-1.2830	-1.2874	1.6	-1.322	-1.3225	0.2
$\Delta C_{M,OH} (x10^2)$	-1.30	-1.2536	15.5	-1.30	-1.2536	15.5	-1.30	-1.2536	15.5	-1.357	-1.2717	16.7
$\Delta \frac{\partial C_M}{\partial x} \alpha_{WCP} (x10^3)$	0.70	2.250	221	0.70	2.307	230	0.70	0.1780	31.7	0.80	-0.3876	148
$C_2 (C.G., 2.5) (x10^4)$	-0.9340	-0.9560	2.1	0.9340	0.9540	2.5	0.9390	0.9470	0.9	-1.003	-1.029	2.6
$\frac{\partial C_M}{\partial x} \hat{x} (x10^4)$	0	0	0	0	0	0	0	0	0	-1.401	-1.386	1.0
$\frac{\partial C_M}{\partial y} \hat{y} (x10^3)$	0	0	0	0	0	0	0	0	0	-1.386	-1.383	0.2
$\frac{\partial C_M}{\partial m_2} m_2 (x10^3)$	-6.033	-5.913	2.0	-5.715	-5.602	2.0	-6.350	-6.229	1.9	-6.350	-6.277	1.0
$\Delta C_{M,SP}$.2006	.2016	0.5	.2410	.2417	0.3	.1564	.1553	0.7	.3560	.3377	5.1
$\Delta C_{M,SC} (x10^4)$	-1.8787	-1.9048	3.0	-1.8175	-1.8405	2.8	-1.9481	-1.9588	1.1	-1.6154	-1.5825	3.3
$\Delta C_{M,EFAR} (x10^2)$	0.350	0.3281	6.3	0.350	0.3118	10.9	0.370	0.3593	2.9	0.150	0.0954	36.1
$\Delta C_{M,SIDESHIP} (x10^2)$	0	0	0	0	0	0	0	0	0	0	-1.1325	—
$\Delta C_{M,RUDDER} (x10^3)$	0	0	0	0	0	0	0	0	0	0	.2091	—
$C_{M,TOTAL}$	-1.2727	-1.2738	0.4	-1.03891	-1.03852	1.0	-1.1261	-1.1380	9.4	-1.1369	-1.1551	13.3

$$* \Delta \frac{\partial C_M}{\partial x} \alpha_{WCP} = \left[\left(\frac{\partial C_M}{\partial x} \right)_M - \left(\frac{\partial C_M}{\partial x} \right)_{M=0} \right] \alpha_{WCP}$$

ORIGINAL PAGE IS
OF POOR QUALITY

Table X
Comparison of the Roll Coefficients
of the Model and the Original Data

	CASE #1			CASE #2			CASE #3			CASE #4		
COEFFICIENT COMPONENT	ORIG. DATA	MODEL	Δ (%)	ORIG. DATA	MODEL	Δ (%)	ORIG. DATA	MODEL	Δ (%)	ORIG. DATA	MODEL	Δ (%)
$\frac{\partial C_L}{\partial \beta} \beta \quad (10^3)$	0	0	0	0	0	0	0	0	0	2.826	2.767	2.1
$\frac{\partial C_L}{\partial \dot{\beta}} \dot{\beta} \quad (10^5)$	0	0	0	0	0	0	0	0	0	-3.424	-3.177	0.7
$\frac{\partial C_L}{\partial \ddot{\beta}} \ddot{\beta} \quad (10^5)$	0	0	0	0	0	0	0	0	0	2.301	2.433	5.7
$\Delta C_{L_{AILERON}} \quad (10^3)$	0	0	0	0	0	0	0	0	0	-1.520	-1.207	20.6
$\Delta C_{L_{RUDDER}} \quad (10^3)$	0	0	0	0	0	0	0	0	0	-1.513	-1.427	2.9
$C_{L_{TOTAL}} \quad (10^4)$	0	0	0	0	0	0	0	0	0	-2.180	1.229	156

Table XI

Comparison of the Yaw Coefficients
of the Model and the Original Data

	CASE #1			CASE #2			CASE #3			CASE #4		
COEFFICIENT COMPONENT	ORIG. DATA	MODEL	Δ (%)	ORIG. DATA	MODEL	Δ (%)	ORIG. DATA	MODEL	Δ (%)	ORIG. DATA	MODEL	Δ (%)
$\frac{\partial C_N}{\partial \beta} \beta$	0	0	0	0	0	0	0	0	0	-2.314×10^{-7}	-2.358×10^{-7}	1.9
$\frac{\partial C_N}{\partial \hat{\alpha}} \hat{\alpha}$	0	0	0	0	0	0	0	0	0	-1.658×10^{-6}	-1.695×10^{-6}	2.2
$\frac{\partial C_N}{\partial \hat{\phi}} \hat{\phi}$	0	0	0	0	0	0	0	0	0	-1.325×10^{-5}	-1.330×10^{-5}	0.4
$\frac{\partial C_N}{\partial \hat{r}} \hat{r}$	0	0	0	0	0	0	0	0	0	-1.616×10^{-5}	-1.619×10^{-5}	0.2
$\Delta C_{N_{RUDDER}}$	0	0	0	0	0	0	0	0	0	6.396×10^{-3}	7.092×10^{-3}	10.9
$\Delta C_{N_{AILERON}}$	0	0	0	0	0	0	0	0	0	-1.320×10^{-4}	-9.381×10^{-5}	40.7
$C_Y (C.G.-.25) \frac{\bar{c}}{b}$	0	0	0	0	0	0	0	0	0	-2.423×10^{-5}	-2.377×10^{-5}	1.9
$C_{N_{TOTAL}}$	0	0	0	0	0	0	0	0	0	6.208×10^{-3}	6.943×10^{-3}	11.8

a small angular acceleration.

$$\Delta a_{roll} = \frac{1}{2} \rho V^2 S b C_1 / I_{xx} \quad (\text{rad/sec}^2) \quad (3.35)$$

Assuming

$$\rho = 2.38 \times 10^{-3} \text{ slugs/ft}^3 \quad (\text{sea level})$$

$$V = 202 \text{ ft/sec}$$

$$S = 980 \text{ ft}^2$$

$$b = 93 \text{ ft}$$

$$C_1 = (1.229 - (-2.18)) \times 10^{-4} = 3.409 \times 10^{-4}$$

$$I_{xx} = 375,000 \text{ slugs-ft}^2$$

then

$$\Delta a_{roll} = 443 \text{ ft-lb/} 375,000 \text{ slug-ft}^2 \quad (3.36)$$

or

$$\Delta a_{roll} = 1.18 \times 10^{-3} \text{ rad/sec}^2 = 0.07 \text{ deg/sec}^2 \quad (3.37)$$

This error in the acceleration is very small. Employing (3.35) with the substitution of

$$I_{zz} = 1,200,000 \text{ slugs-ft}^2$$

$$C_n = (6.943 - 6.208) \times 10^{-3} = 7.35 \times 10^{-4}$$

for I_{xx} and C_1 , respectively, gives the yaw acceleration

$$\Delta a_{yaw} = 3253 \text{ ft-lb/} 1,200,000 \text{ slugs-ft}^2 \quad (3.38)$$

or

$$\Delta a_{yaw} = 2.7 \times 10^{-3} \text{ rad/sec}^2 = 0.16 \text{ deg/sec}^2 \quad (3.39)$$

This error is also small. Therefore, the model accuracy for all three moment coefficients is acceptable.

3.9) Summary

The aircraft model was developed utilizing least-squares polynomials approximating the stability derivatives for a Boeing 737. Fourier cosine series were also applied, but only for five derivatives. In addition to modeling the derivatives, the aircraft's state and control constraints were also included. The state constraints were enforced either by constants or piecewise polynomials. At each discrete time point the control vector was compared to the constraints and adjusted to insure compliance, if necessary. Both magnitude and rate constraints on the controls were considered.

A number of checks were conducted on the model to verify its correspondence to the actual aircraft response characteristics. In all of these tests, the calculated aerodynamic forces and moments in the model closely paralleled those of the actual aircraft.

IV. PROGRAMMING THE STEEPEST DESCENT OPTIMIZATION PROCEDURE

4.1 Introduction

The annual report [2] submitted a year ago summarized the mathematics involved in the steepest descent procedure. The equations now have all been programmed and apparently debugged.

4.2 Problem Areas

During the first attempts to run the program, several problems arose. One was related to the passenger comfort model. A measure of passenger discomfort had been normalized to unity and then raised to the power of one hundred. If there was passenger discomfort, then the indicator would exceed unity and, when raised to the power of one hundred, would be extremely large. Likewise, when the indicator was less than unity, the quantity raised to the power of one hundred would be extremely small. This type behavior was thought to be desirable for use as a penalty function to be included with the performance index; however, when there was discomfort, the indicator raised to the power of one hundred became so large that it exceeded the handling capacity of the computer. It was then decided to raise the indicator to the power of ten if the indicator exceeded unity and to the power of one hundred if the indicator was less than unity. This seemed to work and still accomplish the objective.

Another area in which we have experienced some difficulty has to do with the stopping condition. Ideally, the optimization procedure should be allowed to pick that terminal time which is optimum for the situation. To allow this freedom a stopping condition must be chosen. As was described in the final report [2] for last year's work, the stopping condition was formulated as the time rate change of distance between the aircraft and the airport. Whenever this distance stopped decreasing and began increasing (i.e. when its time rate of change went through zero), the trajectory would terminate. Theoretically, successive iterations would cause this event to occur closer and closer to the desired boundary conditions. In order to prevent over-restricting the maneuver, it was decided to begin testing for the stopping condition only after the aircraft had gotten within five miles of the airport.

The net result was that the aircraft seemed to seek out areas of low population density and circle over these areas. This would continue until the upper limit on computer time was reached at which time the trajectory was terminated. Attempts to resolve this problem by additional emphasis on boundary condition errors and time helped somewhat but did not cure the problem. It was then decided to switch over to a fixed-time approach. The time required for a straight-in constant-glide-slope trajectory was calculated. This time was increased by twenty percent to allow time for curves in the trajectory. The problem was then run as one of fixed time.

4.3 Program Size and Cost

As one would guess, the program for performing the optimization is quite complex and lengthy. The total storage requirements vary, depending on the length of the trajectory to be optimized. For a 500-second trajectory (20 miles) the storage requirements are 41×10^3 words. The total computation time per iteration for a 500-second trajectory is 750 seconds. Note that this includes not only the aircraft equations of motion but the evaluation of the noise effect every five seconds and also the backward integration of three sets of adjoint equations. The total computing cost per iteration for a 500-second trajectory is \$40. We presently estimate that twenty iterations may be required to converge to the optimal solution. This comes to \$800 per optimal trajectory. The entry point into the near terminal area is variable, and there are four runways which can be used for landing. Thus, optimal trajectories for several sets of boundary conditions need to be calculated. The next section discusses the results obtained so far.

V. RESULTS

5.1 Introduction

The utility of a performance index for comparing various trajectories is apparent and has been discussed in some detail in the report [2] of our work in 1974-75. There, we reported comparisons of three-degree glide-slope trajectories with six-degree glide-slope trajectories.

Since that time, we have been able to implement the optimization procedure and allow it to search for the optimal trajectory. We began with a one-hundred second trajectory (approximately four miles). The initial trajectory was straight in at a glide slope of three degrees. Table XII lists the results of ten consecutive iterations.

The quantity J is the performance measure. It is given by the equation

$$J = .7 \times \text{Time(sec)} + .05 \times \text{Fuel(lbs)} + .0001 \times \text{Noise(People-sec)}$$

The next column lists $.25 \, d\psi$, where $d\psi$ is the error in boundary conditions. This consists of

$$\begin{aligned} d\psi = & .25x(X - X_f)^2 + .25x(Y - Y_f)^2 + .25x(Z - Z_f)^2 \\ & + 625x(\gamma - \gamma_f)^2 + 5000x(\psi - \psi_f)^2 \end{aligned}$$

where X , Y , and Z represent the coordinates of the aircraft at final time, and X_f , Y_f , and Z_f represent the desired values for these coordinates. The angle γ is the flight path

ITERATION	J	$0.25 \times d\psi$	ΔJ_{PRED}	$X_F(\text{ft})$	$Y_F(\text{ft})$	$h_F(\text{ft})$	$\gamma_F(\text{deg})$	$\psi_F(\text{rad})$
				-6976	5654	409	-2.75	-0.60
1	103.0	$.2947 \times 10^6$	+ 7.62	-5,248	4,476	993	-2.41	- .60
2	107.6	$.7795 \times 10^7$	+ 0.25	-16,539	- 91.6	815	-5.41	-2.50
3	108.2	$.3979 \times 10^7$	- 0.52	-12,222	- 343	790	-5.52	-1.67
4	106.9	$.2324 \times 10^7$	- 1.37	-10,013	380	739	-5.45	-1.29
5	103.7	$.1341 \times 10^7$	- 1.98	- 8,812	1,414	695	-5.45	-1.38
6	99.7	$.7498 \times 10^6$	- 2.21	- 8,244	2,446	651	-5.48	-1.61
7	96.6	$.4307 \times 10^6$	- 1.30	- 8,320	3,418	592	-5.32	-1.91
8	94.8	$.2698 \times 10^6$	- 0.85	- 8,509	4,278	502	-5.10	-2.16
9	93.3	$.1620 \times 10^6$	- 0.83	- 8,388	4,923	402	-4.61	-2.26
10	92.0	$.14089 \times 10^6$	--	- 8,428	5,896	289	-4.14	-2.41

Table XII

Results of Ten Iterations on A Four-Mile Trajectory

angle, and ψ is the heading angle.

5.2 Pattern of Convergence

One important feature to note is that J the performance measure decreased monotonically after the third iteration. Also, the boundary condition error, $d\psi$ decreased monotonically after the second iteration. The predicted change in performance, ΔJ_{PRED} always had the correct sign and, in most cases, was quite close in magnitude. This closeness is a measure of the degree with which the linearity assumptions are being met. If these assumptions are grossly violated, there is no guarantee of convergence toward an optimum. To ensure linearity one must keep the step size from one iteration to the next sufficiently small. Our program automatically reduces the allowable step size to one half its previous value if the performance measure ever increases. So far, this strategy seems to be working satisfactorily.

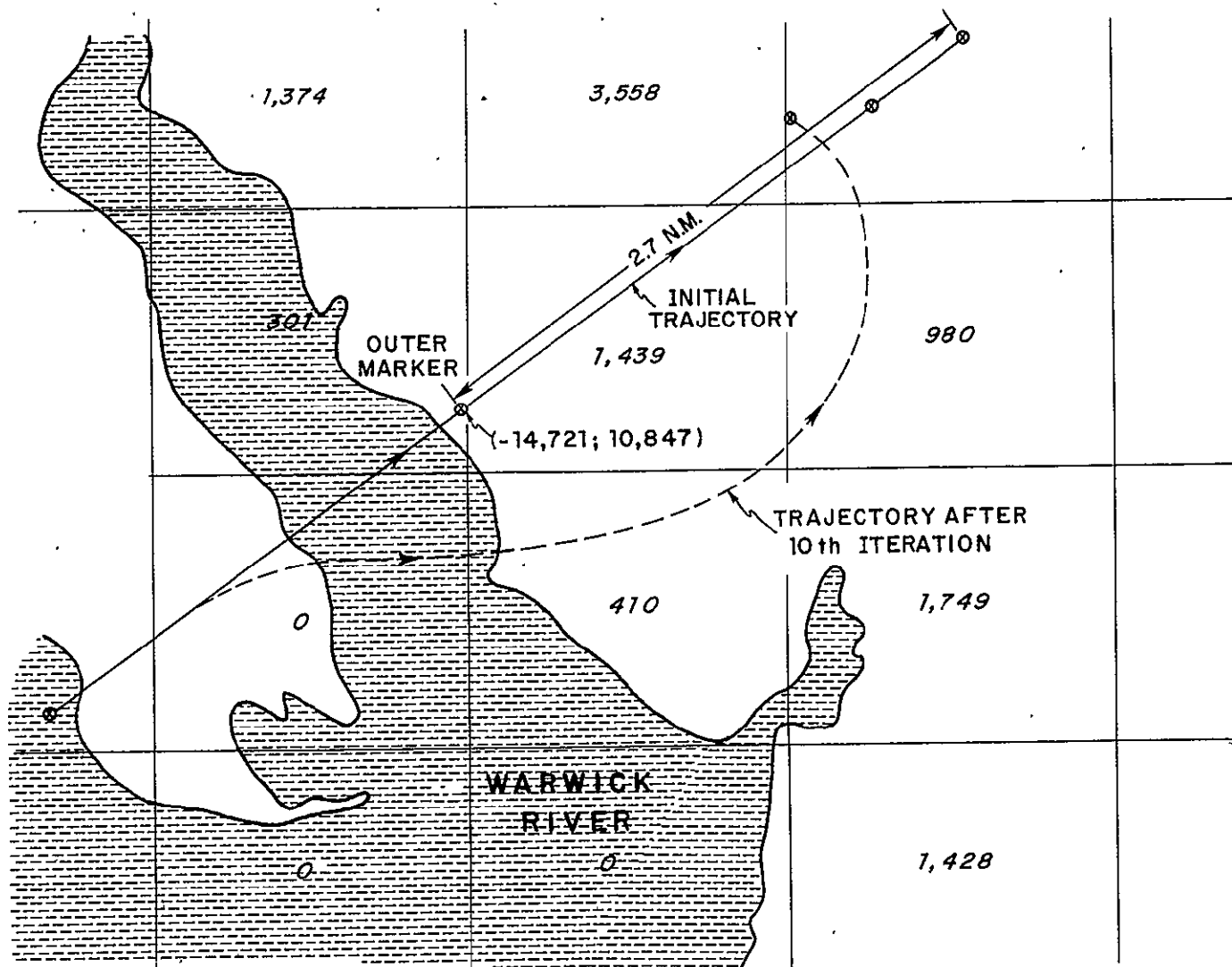
Examining once more the column on performance index, J it appears that reducing the value from 103 to 92 is not all that significant. However, recall that we are now working with a fixed time problem which means that a portion of J , $.7 \times 10^4$ seconds, is fixed. The variable portion of the performance measure actually decreased from 30 on the first iteration to 19 on the tenth iteration. The noise component decreased from 21 to 11. Thus, a significant improvement has been achieved.

Judging from $d\psi$, it is apparent that the convergence is not complete, i.e. the boundary conditions have not been

completely satisfied. Figure 5.1 illustrates this also. However, it is believed that additional iterations would bring these boundary condition errors closer to zero. On Fig. 5.1 it is seen that the trajectory for the tenth iteration is one which swings across the areas of low population density and cuts between the two areas of high population density. This is as one would hope the procedure would work. Hopefully, additional iterations would change the curvature at the very end of the trajectory and make the final heading of the aircraft toward the runway.

The four-mile trajectory is actually not a realistic problem, although it does seem to prove out the workability of our program. Such a short trajectory does not allow room for very much maneuvering or time to recover from the maneuver and align with the runway. By going to the twenty-mile trajectory, more freedom will be given to the procedure; and the areas of low population density may be sought out while still affording time for the aircraft to straighten out for the final approach to the airport. A shortage of computing funds precluded the optimization of any twenty-mile trajectories this past year.

Figure 5.1
Results of Ten Iterations
on a Four-Mile Trajectory



VI. CONCLUSIONS AND FUTURE PLANS

At this point all our models have been developed and programmed, and our procedure is working. There is still a certain amount of art as well as science involved in the successful use of the procedure. Convergence is very much a function of the initial guess and the step size. Furthermore, a step size which works for awhile may cause oscillation later and have to be reduced. In some cases automatic reduction of step size has been successful; however, in general a certain amount of user interaction seems to be a necessity.

The results we have obtained for the four-mile trajectory are very encouraging. Things seem to be behaving as one would expect. We are most anxious to begin applying our program to the twenty-mile trajectories. There are several sets of boundary conditions for which we desire optimal trajectories. If possible, we would also like to investigate the sensitivity of the optimal trajectories to changes in the values of the weighting parameters in the performance index. The inclusion of wind in our simulation is a possibility. One other item which may be worth considering is the frequency of landings as opposed to treating each landing separately.

VII. REFERENCES

1. Cook, G., Witt, R. M., and Barkana, A., "Research Studies in the Area of Optimal Landing Flight Path Trajectories," NASA Contract No. NAS 1-10210, Task Order No. 8, U.Va. Report No. EE-4038-101-74, Dec. 1974.
2. Cook, G. and Witt, R. M., "Optimization and Sensitivity Studies of Flight Path Trajectories," NASA Contract No. NSG 1101, U.Va. Report No. EE-4038-102-75, Sept. 1975.
3. Barkana, A., and Cook, G., "An Aircraft Noise Pollution Model for Trajectory Optimization," IEEE Trans. on Aerospace & Electronic Systems, Vol. AES-12, No. 2, March 1976.
4. Witt, R. M. and Cook, G., "A Performance Measure for Evaluating Noise Effects During Landing," submitted to IEEE Trans. on Aerospace & Electronic Systems.
5. Aerodynamic Data for the 737 Flight Simulator, Boeing Document No. D6-58123, rev.F.
6. Etkin, B., Dynamics of Atmospheric Flight, John Wiley & Sons, Inc., NY, 1972.
7. Rosko, J. S., Digital Simulation of Physical Systems, Addison-Wesley Publishing Co., Reading, MA, 1972.
8. Va. 1976-77 Airport Directory, Div. of Aeronautics, St. Corp. Commission, Richmond, VA, 1976.
9. Kuethe, A. M. and Schnetzer, J. D., Foundations of Aerodynamics, John Wiley & Sons, Inc., NY, 1967.
10. JT8D Commercial Installation Handbook, Pratt & Whitney Aircraft, Aug. 27, 1970.

DISTRIBUTION LIST

Copy No.

1 - 2	NASA Scientific & Technical Information Facility P. O. Box 8757 Baltimore/Washington International Airport Maryland 21240
3 - 5	Mr. R. M. Hueschen Mail Stop 473 NASA/Langley Research Center Hampton, Virginia 23665
6 - 7	G. Cook
8 - 9	R. M. Witt
10	J. N. Warfield
11	I. A. Fischer
12 - 13	E. H. Pancake Clark Hall
14	RLES Files

UNIVERSITY OF VIRGINIA

School of Engineering and Applied Science

The University of Virginia's School of Engineering and Applied Science has an undergraduate enrollment of approximately 1,000 students with a graduate enrollment of 350. There are approximately 120 faculty members, of whom, about 90% hold a doctorate. Excellence in graduate education is aided and supplemented by a research program approximating \$3 million per year. This relatively high level of participation in sponsored research is one factor which helps our faculty consistently to maintain high quality graduate education at all degree levels.

As research is an integral part of the educational program, research interests parallel academic specialties. These interests range from the traditional engineering departments of Chemical, Civil, Electrical and Mechanical to include departments of Biomedical Engineering, Engineering Science & Systems, Materials Science, Nuclear Engineering, and Applied Mathematics & Computer Science. In addition to these departmental interests, there are interdepartmental groups in the areas of Automatic Controls and Applied Mechanics. All departments are authorized to offer the doctorate while the Biomedical and Materials Science Departments are graduate degree granting departments only.

The School of Engineering and Applied Science, is an integral part of an outstanding University, which has strong professional Schools of Law, Medicine, and Business Administration. In addition, the College of Arts and Sciences has strong basic science departments in Mathematics, Physics, Chemistry, and other departments relevant to the engineering research program. This not only provides an excellent scholarly climate, but also enhances the school's potential for creating truly interdisciplinary teams in the pursuit of our basic goals of education, research, and public service.

Inside this cover are listed some of the present research activities of the department from which this report originates. For more information on this or other areas, address the department chairman or Dean J. E. Gibson, Commonwealth Professor and Dean, School of Engineering and Applied Science, University of Virginia, Charlottesville, Virginia 22901.